Coupled Numerical Simulation of Liquid Sloshing Dampers and Wind-Structure Simulation Model

Victor Vîlceanu*, Igor Kavrakov, Guido Morgenthal

Bauhaus University Weimar, Institute of Structural Engineering, Chair of Modelling and Simulation of Structures, Marienstraße 7, 99423 Weimar, Germany

Abstract

Long-span bridges, high-rise buildings, chimneys, or wind turbines are often susceptible to wind-induced vibrations due to their high flexibility and lightweight. Therefore, these structures should be carefully designed to sustain the wind loads. Employing robust solutions for vibration mitigation, such as tuned liquid dampers (TLDs), enables energy dissipation at reduced structural and maintenance costs. This study presents a numerical coupling methodology for evaluating the wind-induced response of slender vertical structures that include a TLD. The methodology is based on coupling a Computational Fluid Dynamics (CFD) model of a TLD, a semi-analytical aerodynamic force model, and a structural model. The coupling is realized in a time-domain fashion by continuously exchanging sloshing forces, aerodynamic forces, and structural response. The highlight is the use of the volume of fluid (VOF) method as a CFD strategy to represent the sloshing damping forces, including an experimental validation. The methodology is applied to (i) a chimney-type structure to mitigate the buffeting and vortex-induced vibrations and (ii) a high-rise building to reduce the acceleration buffeting response for human comfort. In both cases, strategy for TLD predesign is employed based on free- and forced-vibration analysis, an equivalent tuned mass damper model, and wind vibrations, respectively. The results of the dynamic analyses show that there is a significant reduction in structural response for both cases. The outcome of this study is intended to showcase the applicability of CFD for TLD predesign and modeling nonlinear sloshing forces during dynamic analysis as an alternative to experiments. Thus, it is intended to serve academics as well as practitioners.

Keywords:
Tuned Liquid Damper (TLD), Numerical coupling methodology, Sloshing CFD Model, Meshgrid method, Aerodynamic Model

1. Introduction

Structures such as long-span bridges, high-rise buildings, chimneys, and telecommunication towers, are designed to sustain wind loads and limit the amplitudes of resulting structural vibrations. Wind-induced phenomena, such as vortex-induced vibration or buffeting, could lead to fatigue in structural elements, serviceability issues, or even failure in extreme cases, such as aerodynamic instability [1, 2]. One of the robust solutions for mitigating wind vibrations is using damper systems that allow adding a frequency-modulated mass system to dissipate energy. Perhaps the most widely used damping systems for structural control are the Tuned Mass Dampers (TMDs) [3, 4]. Unlike TMDs, Tuned Liquid Dampers (TLDs) relying on sloshing forces to dissipate energy have shown increased usage in structures due to low maintenance. The application of sloshing motion on structures, such as large elevated water tanks, was investigated as a consequence of ground motion excitation due to earthquakes. Pioneering research studies on the sloshing dynamics and interaction between the structure and the water mass movement have been introduced in the

*Corresponding author, Tel.: +49 3643 584433
Email address: victor.vilceanu@uni-weimar.de (Victor Vîlceanu)

studies of Housner, and Ifrim [5, 6]. More recently, these liquid dampers have been investigated by several authors to suppress wind-induced vibrations, such as the cases for tall buildings [7, 8], or towers [9]. Furthermore, the use of liquid dampers for mitigating multihazard responses can be investigated through use of neural network models, to check dampers performance [10]. Studies have been made for enhancing energy dissipation for liquid dampers through optimal shaping and use of 3D-printing technologies for adjusting the bottom shape for rectangular liquid tanks [11].

The TLDs are comprised of a rigid tank of length (L) with liquid inside up to the height (h_w). The sloshing frequency of the liquid can be expressed from the h_w/L ratio (see fig. 1). This ratio represents a criterion approximation that shows whether TLD is within categories of (i) shallow- and intermediate-liquid ($h_w/L \lesssim 0.2$) or (ii) finite liquid depths ($0.2 \lesssim h_w/L \gtrsim 1$) [12]. The sloshing forces, and thus, the additional damping, depend on other factors such as oscillation amplitude, tank geometry, and boundary roughness.

From an analytical point of view, it is challenging to describe the behavior of the sloshing in the resonance range because of the nonlinearities that the liquid exhibits, particularly in the case of complex geometrical configurations for the liquid containers [13]. Semi-analytical models based on experimental data are introduced [14, 15], wherein the models are based on shallow water theory. Equivalent mechanical models of the liquid dampers were considered as dynamic parameters for design purposes [16]. Several studies developed nonlinear mechanical models based on equivalent TMD, where the nonlinear behavior of the TLD under large excitation amplitudes is captured by the nonlinear stiffness [17, 18].

To overcome the complexity in assessing the characteristics of the sloshing behavior and its associated nonlinearities, computational fluid dynamics (CFD) techniques can provide a physical understanding given the fluid governing laws. CFD methods have proven to be a reliable modeling strategy for sloshing involving breaking-wave phenomena [19], and surface tension for resolving free surface [20]. Cavalagli [21] presented an experimental and numerical study in which the Volume of Fluid (VOF) model is used for TLD to investigate the sloshing phenomenon and to determine the energy dissipation associated to the force-displacement cycles. The use of the VOF method has been shown to study the pressure variations, and the sloshing effects in a moving rectangular tank have been shown [22]. The VOF method using two-phase analysis is shown for tracking free surface phenomenon under the motion of the liquid inside of a tank [23]. Particularly, VOF methods have shown success in modeling the sloshing behavior of ships [24], in which the coupling effect in the time domain is studied between the ship motion response and the sloshing flow. A robust CFD model alternative used for sloshing behavior in a tank under external excitation is based on Smoothed Particle Hydrodynamics (SPH) [25]. Green [26] presented the SPH formulation to simulate long-duration sloshing in partially filled tanks of arbitrary shapes.

Study on structural control using a TLD-SPH model has been coupled with a single-degree-of-freedom (SDOF) structure [27], which was shown the numerical effect of the sloshing absorber for performance control. Hybrid simulations for coupling efficiency of the TLD with the scaled structural properties are shown with feedback in real-time for various external excitations, including wind loading [28]. While the aforementioned studies focus on providing an accurate model for TLD behavior under a given excitation response, there is a lack of research on the efficiency of the TLD for wind-structure interaction, by using a numerical coupled wind-structure-TLD approach, under broadband and resonant response. VOF model for sloshing behavior has the advantage of capturing the nonlinear sloshing dynamics, compared to other simplified or reduced-order models. Whereas physical experiments coupled with virtual system models can replicate the sloshing behavior accurately, one disadvantage could be the costs for large-scale tanks and changes in the geometry, to which CFD-VOF models can be easily adapted.

This paper presents a framework for weakly numerical coupling approach of the fluid-structure-interaction model. The standard analyses in TLD behavior are either composed of (i) mechanical models that tend to replicate the sloshing behavior under given excitation, or (ii) physical experiments at small-scale, or at large-scale with subsequent expensive costs. The transient and fast-changing dynamics of sloshing is of importance, particularly for non-periodic excitation. Therefore, an interaction coupled analysis is proposed for TLD performance under both periodic and non-periodic excitation, to showcase the uni-directional coupled response. Although a 2D-simulation represents a simplification, the advantage of the 2D-CFD sloshing model allows for lower cells discretization with consequences for low computational demands, yet fast and accurate simulations. The methodology is comprised of three models: i) structural model, ii) aerodynamic force model, iii) CFD sloshing model based on VOF. The CFD sloshing model was validated with shaking-table experiments, based on sinusoidal inputs. Further validation with a broadband excitation of the tank would also add and enhance the presented framework. The modelling of TLD is designed to attenuate the

wind response due to (i) buffeting (broad band frequency spectrum), and VIV (single resonant frequency). However, in the current study, VIV model considers vortex shedding described linearly, as a harmonic force exerting along a correlation length, not being able to reproduce the lock-in conditions accurately. The coupled approach was shown for a uni-directional case to highlight the coupling between wind model - structure -TLD model. However, the multidirectional wind responses of the structure have not been addressed, but this could be a future framework study analysis.

In particular, the novel aspects of the presented methodology are:

i. A weakly-coupled partitioned approach between three models for analyzing the wind-induced response of slender structures equipped with TLD.
ii. The coupling with VOF model of a TLD to directly compute feedback sloshing forces during a time-domain simulation of the dynamic response of a structure subjected to transient forces.

First, the numerical coupling framework is introduced in section 2 by defining the three models and an equivalent TMD model. Then, in section 3 we validate the CFD sloshing model with a shaking-table experiment. Section 4 represents the numerical analyses, including TLD predesign on the basis of shallow liquid assumption and tuning criterion, free- and forced-vibration tests for an optimum TLD configuration, an analogy between TLD and equivalent TMD for the forced response, and the wind-induced response of a chimney equipped with TLD, and equivalent TMD, respectively. Section 5 represents the numerical analyses, including TLD predesign and the wind-induced response of a high-rise building equipped with TLD, and TMD, respectively. Finally, conclusions are presented based on the case studies and an outlook for further development.

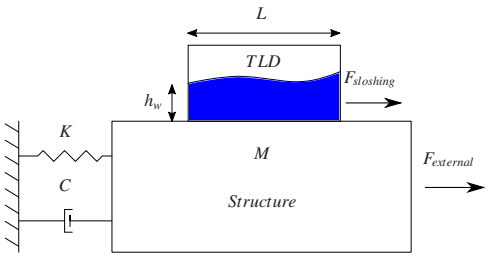

Fig. 1. Schematic of an SDOF system: mass (M) - spring (K) - dashpot (C), equipped with TLD, under external excitation with subsequent action of sloshing forces.

2. Numerical coupling methodology

The coupling methodology is shown in fig. 2, where the framework is exemplified through a study case of applying TLD on a structure subjected to buffeting forces. The methodology is comprised of three distinct models: (i) Aerodynamic Model, (ii) Structural Model, and (iii) TLD Sloshing Model. The structural model is characterized by low structural damping and is discretized on finite elements. The aerodynamic model describes the wind forces acting on the structural model based on wind properties characteristic of the site. Finally, the sloshing model is solved by using CFD and the displacement at a specific node where the TLD is positioned.

Once the setup (problem definition) for the simulation has been created, the numerical time integration is displacement-controlled by the two-way coupling between the (i) structural and aerodynamic model and (ii) structural and CFD model. The structural displacement response for the node where TLD is applied to the tank in CFD solver exciting the tank; thus, the net sloshing force is obtained and updated as an external force vector in the equation of motion. The schematics in fig. 2 show the structure based on discrete information, wind profile characteristics, and liquid damper. In this way, the coupled analysis is sequentially performed, and the time-history response of discrete nodes can be evaluated. For example, the schematic for buffeting analysis shows the TLD applied at the top node (”n”), in which the sloshing force is considered at the respective node.

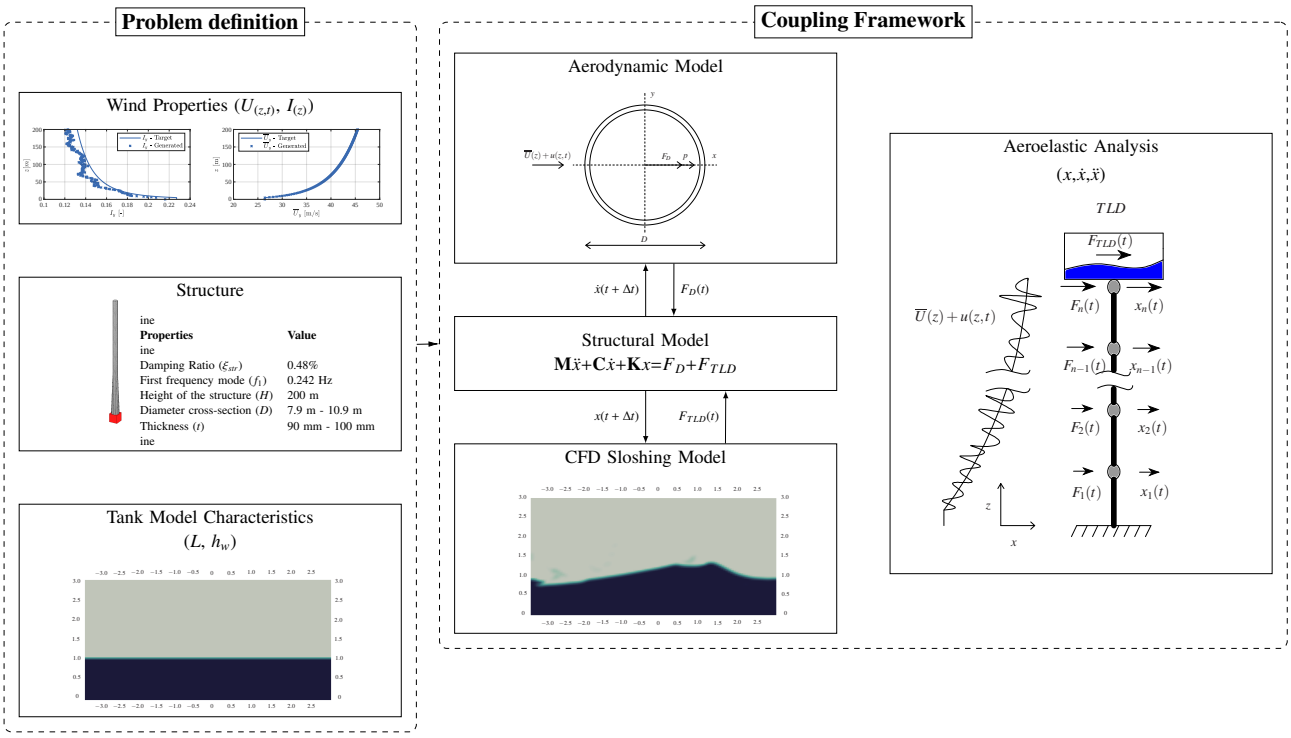

Fig. 2. Framework example of the coupling method between the TLD and chimney model under buffeting wind response.

2.1. Structural Model

The equation of motion describes the structural model with particular structural properties in terms of mass, damping, and stiffness (1). The structure is solved in the mode space, thereby reducing it to its intrinsic dynamic properties. The generalized equation for the dynamic analysis under a given external force is (1),(2.1) [29] :

$$\mathbf{M}^*\ddot{\mathbf{x}} + \mathbf{C}^*\dot{\mathbf{x}} + \mathbf{K}^*\mathbf{x} = \mathbf{f}^*, \tag{1}$$

$$\begin{aligned} \mathbf{M}^* = \mathbf{\Phi}^T\mathbf{M}\mathbf{\Phi}, \quad \mathbf{C}^* = \mathbf{\Phi}^T\mathbf{C}\mathbf{\Phi}, \quad \mathbf{K}^* = \mathbf{\Phi}^T\mathbf{K}\mathbf{\Phi} \\ \ddot{\mathbf{x}}^* = \mathbf{\Phi}^T\ddot{\mathbf{x}}, \quad \dot{\mathbf{x}}^* = \mathbf{\Phi}^T\dot{\mathbf{x}}, \quad \mathbf{x}^* = \mathbf{\Phi}^T\mathbf{x}, \quad \mathbf{f}^* = \mathbf{\Phi}^T\mathbf{f}, \end{aligned} \tag{2}$$

where $\mathbf{M}$, $\mathbf{C}$ and $\mathbf{K}$ are mass, damping, and stiffness matrices, respectively; $\ddot{\mathbf{x}}(t)$, $\dot{\mathbf{x}}(t)$ and $\mathbf{x}(t)$ are the accelerations, velocities, and displacements, respectively, with respect to time; $\mathbf{f}$ is the external force vector; $\mathbf{M}^*$, $\mathbf{C}^*$ and $\mathbf{K}^*$ are the generalized mass, damping, and stiffness, respectively, associated to its correspondent mode shape $\mathbf{\Phi}$; $\mathbf{f}^*(t)$ is the generalized external force; $\ddot{\mathbf{x}}^*(t)$, $\dot{\mathbf{x}}^*(t)$ and $\mathbf{x}^*(t)$ are the generalized accelerations, velocities, and displacements, respectively, with respect to time.

The generalized equation can be targeted for a specific mode of vibration, as in our example analysis, in which case the mode shape, $\mathbf{\Phi}$, becomes a vector.

The structure is modeled with FE method, with unit elements to which nodal forces are applied based on the examined excitation type (buffeting, harmonic force, equivalent VIV model). For example, the buffeting case (depicted in fig.2) considers the wind forces from the wind profile as correlated load along the MDOF structure in nodes. In the case of harmonic force only, the case is simplified to basically a SDOF system with a force load acting on it, since the harmonic load is applied to the tip of the structure.

2.2. Aerodynamic Model

In this article, two different aerodynamic models are studied to describe the wind-induced phenomena: (1) quasi-steady model for buffeting analysis and (2) harmonic VIV-like model for vortex-induced forces (Eurocode: EC1-4:2010). The fluctuating wind speed brings unsteady effects to slender and flexible structures with a low damping ratio [30],[31]; therefore, a buffeting analysis is required to evaluate the dynamic structural response [32]. Furthermore, the free-stream turbulence translates into aerodynamic forces on the structure, leading to unwanted excessive vibrations; thus, liquid dampers can provide a long-term solution for suppressing these vibrations.

The wind-structure interaction can be expressed through the equation of motion by considering the wind force (**f**) on the right-hand side. The aerodynamic force model is a quasi-steady model, which considers an equivalent steady-state at each time step for the forces from the fluid-structure interaction [33, 34].

The static wind coefficients for complex structures are determined in the wind tunnel tests; for the present application of circular section, validated and standardized values are used [35]. The present article focuses on the TLD under uni-directional excitation along with wind for buffeting cases. The drag force, F_D, according to the linear quasi-steady model, is described as follows:

$$F_D = \frac{1}{2}\rho U^2 D\left[C_D + 2C_D\frac{u}{U} - 2C_D\frac{\dot{p}}{U}\right], \tag{3}$$

where ρ is the air density (1.25 kg/m^3), U is the mean wind velocity, D is the width of the section, C_D is the drag coefficient, u is the fluctuating wind speed, and $\dot{p}$ is the relative velocity within the term which expresses the aerodynamic damping. The limitations of quasi-steady assumption entail the dismissal of fluid memory or nonlinear unsteady aerodynamic damping.

The mean wind speed in the atmospheric boundary layer is described through the wind profile. Here, the logarithmic profile is used [36] for a uniform roughness over a sufficiently large fetch. The fluctuating component u is assumed to be stationary and Gaussian. It is characterized by the turbulence intensity I_u and its spectra, which is assumed to follow the von Karman model with Vickery's coherence model [37]. Based on these turbulent properties, time-histories of the turbulent component $U(t)$ are simulated along the height by sampling a correlated random process [38]. Each time history is 10 minutes long, which is usually considered sufficient for applications in wind engineering.

The second aerodynamic model used is for modeling VIV, which is usually relevant for serviceability limit state checks in terms of limiting displacements and accelerations. Vortex sheddings occur whenever a structure is subjected to wind vibrations, which could potentially produce larger displacements if the vortices shed with a frequency close to the natural frequency of the structure. The goal is to show the effectiveness of TLD for VIV-like excitation by determining the cross-wind amplitudes accounting for vortex shedding. To this purpose, we have presented a simple harmonic forcing formula, which can approximate the vortex shedding based on empirical formulas.

The vortex shedding action can be expressed as the inertia force acting perpendicular to the wind direction along with a certain correlation height of the structure:

$$F_w(z) = m(z)(2\pi f_i)^2\phi_i(z)y_{max}, \tag{4}$$

where $m(z)$ is the vibrating mass per unit length [kg/m], f_i is the frequency of the structure of the i^{th} mode with its associated mode shape, ϕ_i, normalized at 1 with respect to the maximum displacement, y_{max}. In this manner, a dynamic analysis accounting for the equivalent VIV force is generated for the first vibration mode. The calculated parameters may be referred to for the study application in fig. 19. A more detailing explanation of the calculation of the equivalent VIV forces is given in the Appendix A.

2.3. Sloshing Model

Sloshing forces in a 2D rectangular tank with rigid walls is described through CFD using the FVM (see fig. 2), simulating the fluid-structure interaction between the water and the tank. The tank consists of two fluids (water and air), with boundary conditions between (a) solid-fluid and (b) fluid-fluid solved through multiphase flows using VOF method. Next, we describe the CFD sloshing model by the (i) governing equations of the fluids, (ii) transport equation at the interface region between water and air, (iii) boundary conditions, and finally, (iv) resultant sloshing forces.

(i) *Governing equations of the fluid*. The fluid flow in a continuum is described as an incompressible and

Newtonian fluid. A set of partial differential equations characterizes the general Navier-Stokes equations describing the balance of mass and momentum:

$$\frac{\partial \rho}{\partial t} + \rho \nabla \cdot \mathbf{v} = 0, \quad \frac{\partial \mathbf{v}}{\partial t} = -\frac{1}{\rho}\nabla P + \nu \nabla^2 \mathbf{v} + \mathbf{g}, \tag{5}$$

where ρ is the fluid density, $\mathbf{v}$ is the velocity, P is the fluid pressure, ν is the laminar kinematic viscosity and $\mathbf{g}$ is the gravitational acceleration.

(ii) *Transport equation at the interface region between the water and air.* We use the Volume of Fluid Method (VOF) [39] to simulate a two-phase flow between air and water. The VOF method solves for two incompressible fluids by phase-fraction interface (α), where $\alpha = 1$ inside fluid 1 (water), having the density ρ_1, and $\alpha = 0$ inside fluid 2 (air) with the density ρ_2. Besides the continuity and momentum equations, another term, i.e.transport equation, represents the volume fraction accounting for the interface region:

$$\frac{\partial \alpha}{\partial t} + \nabla(U\alpha) = 0, \quad \rho = \alpha\rho_1 + (1-\alpha)\rho_2. \tag{6}$$

The phase-fraction interface coefficient, α, varies between 0 and 1 at the interface between the two fluids. In this way, the two fluids are considered adequate throughout the domain. The physical properties are calculated as weighted averages based on the distribution of liquid volume fraction, thus being equal to the properties of each fluid in their corresponding occupied regions and varying between 0 and 1 across their interface. Therefore, the interface region must have a high number of cells to produce reliable results for the surface tension [40]. The latter generates an additional pressure gradient, for which a surface force (f_σ) model [20]:

$$f_\sigma = \sigma\kappa\nabla\alpha, \quad \kappa = -\nabla\Big(\frac{\nabla\alpha}{|\nabla\alpha|}\Big), \tag{7}$$

where κ is the mean curvature of the free surface, σ is the surface tension constant.

(iii) *Boundary conditions.* The boundary conditions around the two-dimensional solid tank domain are: (1) $\mathbf{n}\nabla\alpha = 0$, $\mathbf{n}\nabla p = 0$, no-slip on the bottom, right, and left walls of the tank, (2) $\alpha = 0$, $\mathbf{n}\nabla\mathbf{v}$, p=0 for the top side of the tank, where $\mathbf{n}$ is the unit normal to the outer surface structure.

(iv) *Sloshing forces.* Following the general manner for calculating the force due to fluid flow, the horizontal component of the sloshing force (F_x) is expressed as:

$$F_{sloshing,x} = \int_s (-P\mathbf{I} + \mu[\nabla\mathbf{v} - \nabla\mathbf{v}^T])\mathbf{n}\mathrm{d}s \cdot i, \tag{8}$$

where s is the internal tank surface, $\mathbf{I}$ is the identity tensor, μ is the dynamic viscosity, and i is the unit vector array for the x-axis component of the sloshing force. The sloshing force in eq. (8) is further referred as F_{TLD}.

(v) Numerical discretization. The Finite Volume Method (FVM) is used for numerical discretization, which describes the continuity equation in an integral form. This is achieved by small control volumes that define the computational mesh. In [41] the equation calculates the fluxes at the faces of each cell, then centered on the volume centroids; thus, the control volume is used for variables, such as pressure or velocity. Interpolated values are multiplied by the normal surface vector to get the fluxes.

Another relevant parameter for the numerical integration is the Courant number (Co), which ensures numerical stability, controlling the solution at each time step.

$$\mathrm{Co} = \frac{U_f \Delta t}{\Delta x}, \tag{9}$$

where U_f is the velocity on the cell face, Δt is the time step and Δx is the distance between cell centres. The simulation are performed using an adjustable time stepping, for which Co is lower than a prescribed maximum courant number ($\mathrm{Co}_{max} = 2$). The transient sloshing behavior is the reason to increase the Courant number larger than one, which is the case for most applications. PIMPLE algorithm is used, which combines Pressure Implicit with Splitting of Operator (PISO) with the Semi-Implicit Method for Pressure-Linked Equations (SIMPLE), to achieve better numerical stability. For the transient problem, it is used steady-state treatment (SIMPLE) to find the steady-state solution for each time

step. To solve the Eq.(5), Gauss linear scheme is utilized. A first-order accurate Euler implicit scheme is used for temporal discretization. The computational domain for the two-dimensional representation is discretized using Hexa-dominant unstructured mesh, in which the maximum linear cell dimension is not bigger than 6 cm. Readers may refer to [42] for further information and use of VOF model coupled with structure dynamics.

2.4. TMD Equivalent Model

In order to provide an alternative to the TLD's efficiency of using passive dampers on structures, equivalent Tuned Mass Dampers (TMDs) are used. TMDs are passive dampers being mechanically activated by a mass (m), spring (k), and dashpot (c). Following on the Den Hartog criterion, the TMD damping ratio (ξ_{TMD}), and the TMD frequency (f_d) can be approximated from the mass ratio (μ). Leung and Zhang [43] proposed TMD optimized parameters given a damped structure modeled as SDOF under random excitation, as follows :

$$\epsilon = \frac{\sqrt{(1+\mu/2)}}{1+\mu} + (-0.5047 + 0.0764\sqrt{\mu}) + 0.6023\mu)\xi_{str}\sqrt{\mu} + 0.3737\xi_{str}^2\mu, \quad f_d = \epsilon f_s$$
$$\xi_{TMD} = \sqrt{\frac{\mu(1+3\mu/4)}{4(1+\mu)(1+\mu/2)}}, \tag{10}$$

where ϵ is the optimum tuning condition, $\mu = m_d \,/\, m_s$, where m_d is the TMD mass, and m_s is the modal mass of the structure, ξ_{str} is the structural damping ratio, f_d is the frequency of the TMD, proportional to structural frequency (f_s).

The system of 2 DOFs is represented by the structure (SDOF) + TMD (composed of m_d, c_d,k_d):

$$\begin{bmatrix} m_s & 0 \\ 0 & m_d \end{bmatrix} \begin{Bmatrix} \ddot{x}_s \\ \ddot{x}_d \end{Bmatrix} + \begin{bmatrix} c_s + c_d & -c_d \\ -c_d & c_d \end{bmatrix} \begin{Bmatrix} \dot{x}_s \\ \dot{x}_d \end{Bmatrix} + \\ + \begin{bmatrix} k_s + k_d & -k_d \\ -k_d & k_d \end{bmatrix} \begin{Bmatrix} x_s \\ x_d \end{Bmatrix} = \begin{Bmatrix} F \\ 0 \end{Bmatrix}, \tag{11}$$

$$k_d = m_d \cdot (2 \cdot \pi \cdot f_d)^2, \; c_d = 2 \cdot \xi_{TMD} \cdot m_d \cdot 2 \cdot \pi \cdot f_d. \tag{12}$$

By properly tuning the TMD characteristics to the dynamic properties of the structure, the TMD provides a relatively straightforward mechanical solution to reduce the structural response. The TMD mass (m_d), and damping (c_d) were optimized with respect to the peak and root-mean-square (RMS) displacements as for results from forced vibration of the SDOF system with TLD (11). The optimization method for finding the TMD parameters, explained in eq. 10, is based on the particle swarm algorithm (PSO) [44, 45], which looks for optimal values to determine the fitness solution (section 4.2.2). The advantage of using the equivalent TMD over TLD is the computational efficiency. At the same time, the disadvantage lies in the linear TMD limitation in capturing the sloshing behavior nonlinearities in a TLD.

2.5. Coupled Equations

The weakly numerical coupling framework is composed of the models mentioned above, with the general equation of motion being described as:

$$\mathbf{M}^*\ddot{\mathbf{x}} + \mathbf{C}^*\dot{\mathbf{x}} + \mathbf{K}^*\mathbf{x} = f_D + f_{TLD}, \quad \ddot{\mathbf{x}} = \ddot{\mathbf{x}}(t), \quad \dot{\mathbf{x}} = \dot{\mathbf{x}}(t), \quad \mathbf{x} = \mathbf{x}(t), \quad \mathbf{f_D} = \mathbf{f_D}(t), \quad \mathbf{f_{TLD}} = \mathbf{f_{TLD}}(t) \tag{13}$$

where $\mathbf{f}_D$ is the time-varying drag force vector based on eq.3, and $\mathbf{f}_{TLD}$ is the time-varying sloshing force vector based on eq.8. To consider the TMD application, $\mathbf{M}^*$, $\mathbf{C}^*$, $\mathbf{K}^*$, are updated with the associated TMD parameters (m_d, c_d, k_d). In fig. 3 a detailed explanation is shown for the stepwise calculation. The drag force is composed of static force (F_{St}), buffeting forces (F_{B}), and self-excited (F_{SE}). The self-excited forces control the aerodynamic damping; thus, the velocity obtained from time integration is updated in the force calculation. In the VOF method, the sloshing force, F_{TLD}, is calculated following the relative displacement of the tank motion. This is achieved by prescribing the tank boundary with an updated motion resulting from the structural response, $\mathbf{x}(t)$. In terms of the finite volume method, the dynamic mesh is updated with a new mesh velocity ($\mathbf{v_m}$) in the convective term of the general transport equation.

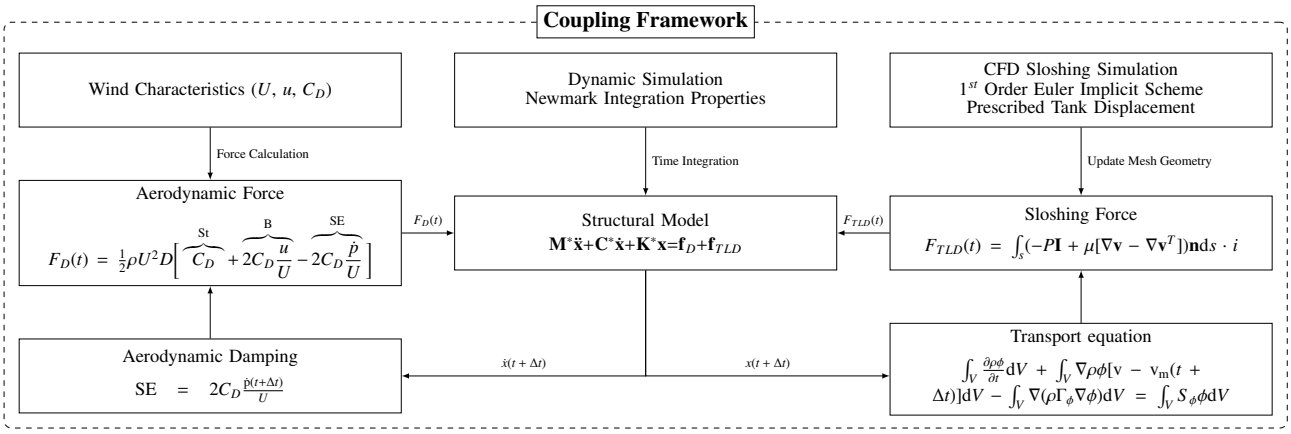

Fig. 3. Overview schematic of the partitioned numerical coupling.

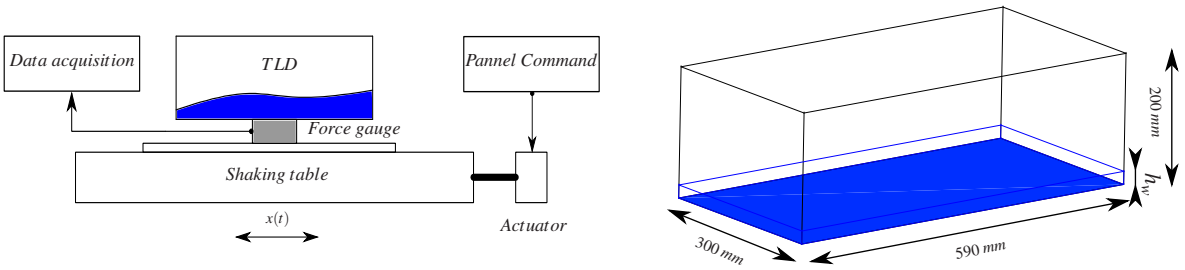

Fig. 4. Left: Schematic of the shaking table experiment for the sloshing tank. Right: Geometrical sketch of the liquid tank.

3. Experimental Validation of the Sloshing Model

A benchmark case for the experiment is used to validate the numerical sloshing method. A rectangular container partially filled with water (see fig. 4 - right) was instrumented on a shaking table to measure the sloshing forces due to external excitation. The experimental setup (see fig. 4 - left) contains a force gauge placed underneath the container, which is connected to data acquisition to provide the horizontal forces measurements.

Since the sensor measures the total inertial forces, a distinction is made to account for the measurements of inertial forces without water (F_i) and the total forces accounting for the tank partially filled with water (F_T).Therefore the sloshing force (F_{TLD}) at each time instant is taken as:

$$F_{TLD} = F_T(t) - F_i(t). \tag{14}$$

The sloshing force is nondimensionalized with respect to the inertial force coming from the liquid mass that does not participate actively in the sloshing [46]:

$$F'_{TLD} = \frac{F_{TLD}}{m_w\omega_e^2 A}, \quad m_w = \rho L b h_w, \quad \omega_e = 2\pi f_e, \tag{15}$$

where m_w is the mass of the liquid at rest, ρ is the density of water (1000 kg/m^3), L is the length of the container (590 mm), b is the width of the container (300 mm), h_w is the height of the water, f_e is the excitation frequency, and A is the amplitude of excitation. The experimental measurements were conducted at a sampling rate of 500 Hz; after that, the low-pass Butterworth 4th order filtering was applied with a cutoff frequency of 1 Hz since the frequencies of interest are within a low range, typically lower than 1 Hz for these liquid dampers.

Given the ratio of the liquid height to the length container (h_w/l), the sloshing frequency (f_{sl}) can be expressed in terms of eigenvalues; thus, each eigenmode is associated with the wave pattern of the surface profile [12]:

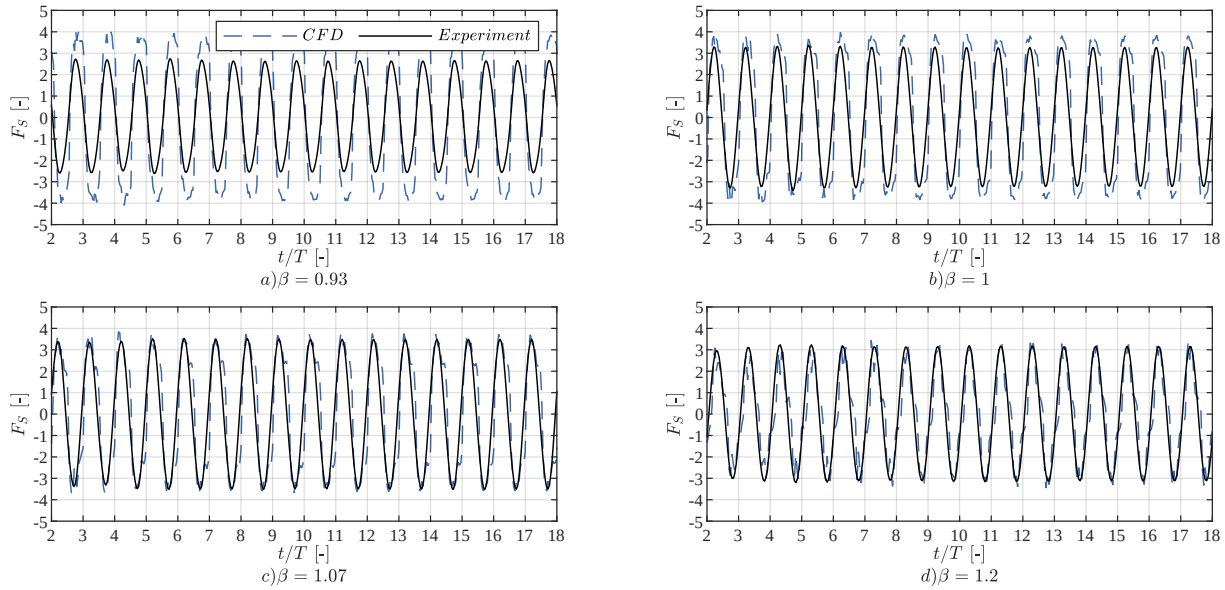

Fig. 5. Nondimensional sloshing forces for the given cases in Table 1 ($\beta = f_e/f_{sl}$). T represents the excitation period for each of the excitation frequencies : a) 0.35 Hz, b) 0.375 Hz, c) 0.4 Hz, d) 0.45 Hz.

ID Case	A [mm]	h_w [mm]	h_w/L [-]	f_e [Hz]	β [-]
a	10	20	0.034	0.350	0.93
b	10	20	0.034	0.375	1.00
c	10	20	0.034	0.400	1.07
d	10	20	0.034	0.450	1.20

Table 1: Measurement campaign for the rectangular container filled with water.

$$f_i = \frac{1}{2\pi}\sqrt{g\frac{\pi i}{L}\tanh\left(\frac{\pi h_w i}{L}\right)}, \tag{16}$$

where i is the mode number, g is gravitational acceleration (9.81 m/s^2).

The lowest natural mode ($i = 1$) is the most significant in the applications of liquid dampers, but higher modes can be activated by tank excitation; thus, vibrations associated with higher structure frequencies can be damped out. Based on the above formulation, represented for the anti-symmetric mode of vibration, the first sloshing frequency is analytically determined. The sloshing frequency from eq.16 is used in all study cases of the coupled analyses using TLD, as a requirement for tuning to the frequency of the structure. The experimental campaign was conducted under different amplitudes (A) and excitation frequencies (f_e). The excitation frequency was set in between the range $\beta(f_e/f_{sl}) = [0.9 - 1.2]$ of the sloshing frequency to capture the resonance and nearly-resonance region, where the liquid container works efficiently as a tuned liquid damper. For validation purposes with the numerical comparison, several cases were considered by varying the excitation frequency as given in Table 1.

As depicted in fig. 5 b), c), and d), the agreement between the experiment and the numerical method for the resonance and near-resonance region shows really good results. However, in fig. 5 a) there are differences in the amplitude, which can be attributed to nonlinearities in the numerical method. The nondimensional sloshing force corresponding to resonance ($\beta = 1$) has slightly bigger amplitudes, as expected, given that the sloshing impact is activated the most. However, within the range of β from 0.93 to 1.2, the force amplitude is close to the maximum one represented for $\beta = 1$. This brings into consideration the frequency range to which the sloshing damper could attain satisfactory results and effectiveness whenever a slight mismatch between the estimation of structural frequency and

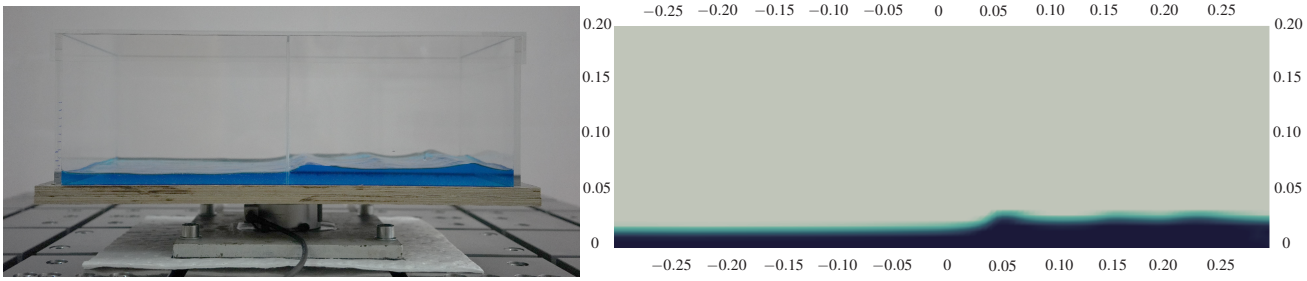

(a) t/T = 3 (left : Experiment setup, right : CFD model).

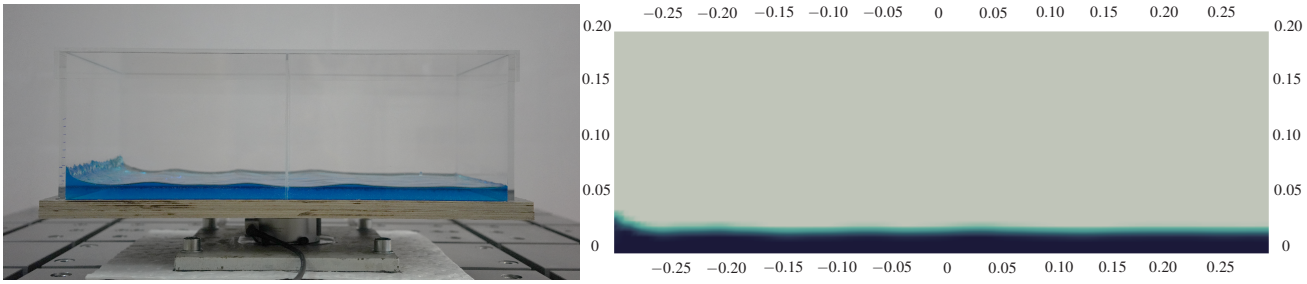

(b) t/T = 3.25 (left : Experiment setup, right : CFD model).

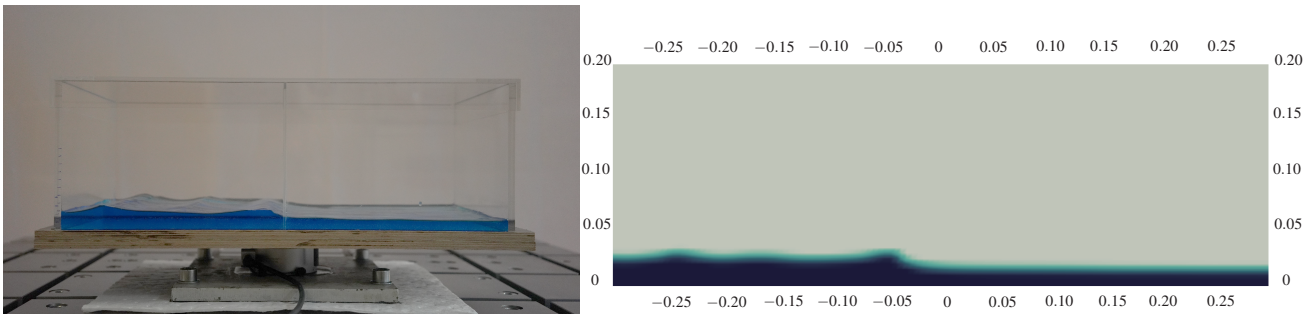

(c) t/T = 3.5 (left : Experiment setup, right : CFD model).

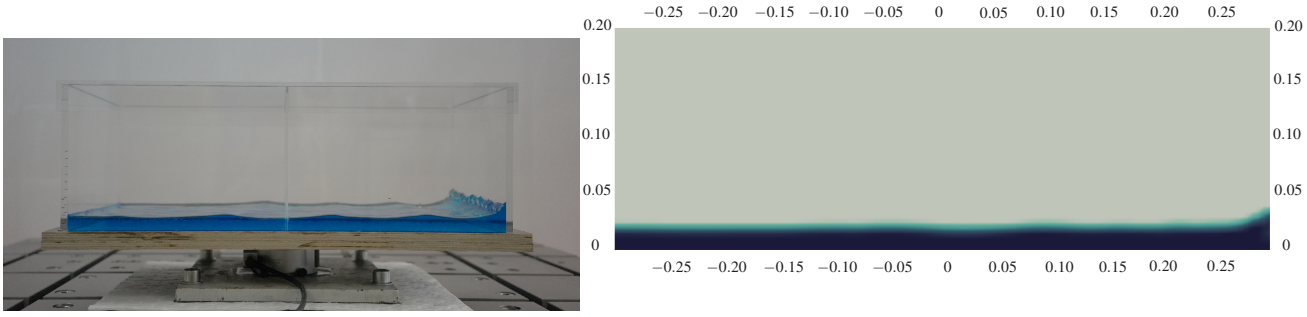

(d) t/T = 3.75 (left : Experiment setup, right : CFD model).

Fig. 6. Time-instant snapshots for the rectangular tank with h_w=20 mm ,excited at f_e=0.375 Hz, with a displacement amplitude of 10 mm.

the sloshing frequency could occur. A lowpass finite impulse response (FIR) filter was applied to the experimental sloshing force at the cutoff frequency of 1 Hz to avoid noise and higher frequency content. The sloshing forces resulting from the CFD model remained unfiltered.

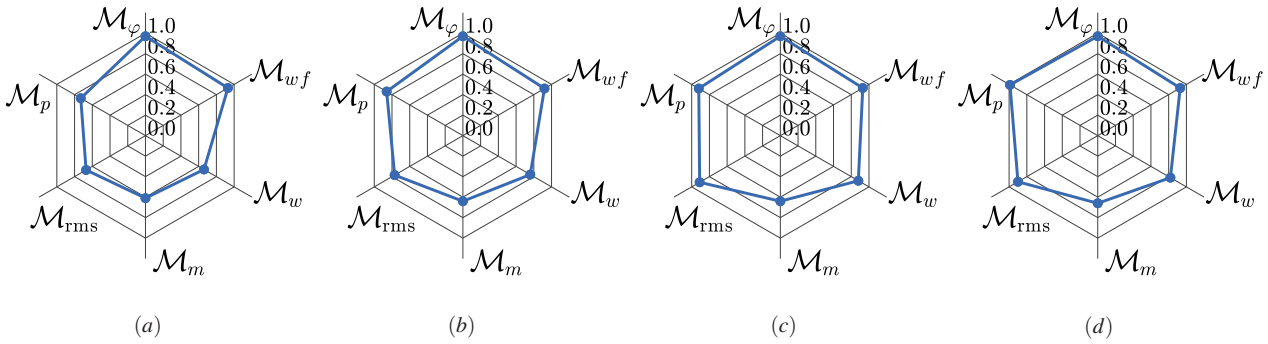

Fig. 7. Comparison metrics for nondimensional sloshing forces between numerical and experimental methods: (a) β=0.93, (b) β=1, (c) β=1.07, (d) β=1.2.

Further quantitative comparison of the time-histories of the sloshing forces is conducted using a unified set of metrics proposed by [47]. Relevant comparison metrics are included to quantify the discrepancies between signal features. The considered metrics used for signal comparison are: phase $\mathscr{M}_\phi$, peak $\mathscr{M}_p$, root mean square (RMS) $\mathscr{M}_{rms}$, magnitude $\mathscr{M}_m$ and wavelet $\mathscr{M}_w$. Each of these comparison metrics is constructed qualitatively using an exponential function with a negative exponent. As such, the metrics attain a value between 0 and 1, where 1 indicates a perfect match and 0 indicates an infinite difference. Generally, a metric ≥ 0.9 is good, showing similar statistical properties. The comparison for each parameter is related with respect to a reference time history which in this case is selected to be the experimental one.

The phase metric $\mathscr{M}_\phi$ shows the mean phase discrepancy between the two-time histories by lag-time correlation. The peak metric $\mathscr{M}_p$ gives the values of sloshing forces relevant to TLD criteria. The RMS metric $\mathscr{M}_{rms}$ is an estimator for the averaged amplitude discrepancies. Magnitude metric $\mathscr{M}_m$ provides differences in a time-localized way. In this regard, preprocessing is applied to align the signals using dynamic time warping, which stretches and aligns the signal without scaling. Finally, the wavelet $\mathscr{M}_w$ provides a 2D representation, in the time and frequency domain, for the time histories. This metric represents the amplitude modulation between two signals, while the $\mathscr{M}_{wf}$ is given by the frequency modulation (see fig. 7). In all the cases, the phase metric ($\mathscr{M}_\phi$), shows an identical match; for the frequency modulation ($\mathscr{M}_{wf}$), the metric is high in all the cases, whereas for others, such as peak ($\mathscr{M}_p$), or RMS ($\mathscr{M}_{rms}$), the metrics are varying from high (cases c,and d) to low (cases b, and a). The magnitude $\mathscr{M}_m$ exhibits lower metric values but is still in a good range.

4. Application: Buffeting and VIV Analysis of a Chimney

4.1. Reference Structure

The selection of a slender structure with low damping and prone to wind vibrations is made to showcase TLD's efficacy for reducing the structural response. To this end, a numerical model is developed from a reference steel chimney [48], having a hollow circular section with varying- cross-section and- thickness along the height. The structural properties are given in fig. 2. The TLDs are primarily targeted for the predominant frequency of the structure (f_{str}=0.242 Hz), where the significant mass of the structure from its total is activated under external actions. The present case shows the effect of TLD for the first frequency of the chimney, which is identified as a horizontal translation from the eigenvalue analysis.

4.2. TLD Predesign

The role of the liquid damper is to be tuned to the structural frequency. The analytical method from eq. (16) provides an evaluation of the sloshing frequency expressed through the following parameters: height of water (h_w) and the length of the container (L) (see fig. 8). Due to the already provided structural frequency, a pair of TLD parameters can be selected to match the specific frequency. This allows us to have an initial estimation of the TLD; however, geometrical constraints shall be considered. The advantage of numerical methods is the possibility of simulations with various sets of parameters to determine the most optimum TLD configuration. By using VOF model, a study is made with several TLD configurations that are following shallow-water criterion, and geometrical constraints, out of

which the optimum configuration is selected.

To this end, a set of free vibration tests are performed for several tanks partially filled with water. Following the shallow water criterion, the frequency of sloshing is chosen to be equal to the frequency of the structure ($\theta = f_{sl}/f_s = 1$). Two other cases are shown in which the sloshing frequency is taken as a lower and higher ratio of the structural frequency. Based on the decay response, their associated damping ratio, and the dynamic reduction, the optimal configuration is selected to be further used in the design. Afterward, forced vibration simulations are performed with the chosen configuration to evaluate the TLD efficacy.

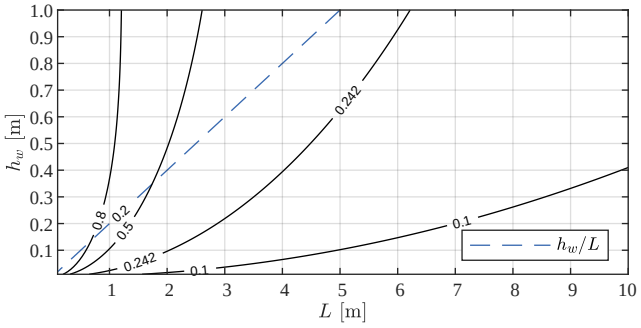

Fig. 8. Sloshing frequency, f_{sl}, (black isolines) for a rectangular tank partially filled with liquid (h_w), given a length (L) (eq. (16)). The dashed blue line represents the threshold defined by the shallow water theory (h_w/L =0.2).

4.2.1. Free-vibration

Configuration	L [m]	h_w [m]	h_w/L [-]	f_{sl} [Hz]	θ [-]	m_{TLD} [kg/m]	ξ_{eff} [%]
1	5.3	0.710	0.134	0.242	1.00	3763	2.6
2	6.3	1.030	0.163	0.242	1.00	6489	3.9
3	7.0	1.300	0.198	0.242	1.00	9100	4.4
4	6.4	0.945	0.147	0.223	0.95	6048	5.3
5	6.4	1.200	0.187	0.254	1.05	7680	3.4

Table 2: Tuned Liquid Damper properties for the resonance (θ=1), and frequency tuning assessment (varying θ).

In order to choose an appropriate tank configuration for the analysis, several configurations of tanks providing the same sloshing frequency are analyzed. This ultimately provides a comparison for masses which can be attributed to sloshing dynamics. The free-vibration tests are performed according to the chimney's first vibration mode with initial displacements. The dynamic characteristics for the first mode of the reference chimney are m_1=356146 kg, k_1=823415 N/m, c_1= 5198 Ns/m. The considered set of parameters for defining the sloshing frequency for the free vibration analyses is shown in Table 2. The damping ratio of the structure (SDOF) is estimated through an envelope curve $A(t) = A_0 e^{-\xi\omega t}$, where A_0 is the initial displacement, ξ is the damping for the enveloppe curve [49]. In order to test the efficiency of TLDs for the free vibration case, two approaches have been used: (i) an exponential curve is fitted through the peaks of the time-history simulation, and an effective damping is determined (ξ_{eff}) (fig. 9,fig. 10), (ii) instantaneous damping is calculated for each of the two succesive peaks, with an average evaluation for the entire time-history ($\xi(t) = 1/[\sqrt{1 + (2\pi/\delta(t))^2}]$, $\delta(t) = \ln[x(t)/x(t+T)]$ [50]). For the former (i), following the above equation, the decaying curves represented by the black dashed line in fig. 9, are associated with effective damping given its time-history response. Since the decaying envelope cannot accurately describe the damping ratio in a fitting curve, given the nonlinear sloshing behavior, the response was evaluated for the first 30 seconds. This provides a reasonably accurate estimation, given the salient nonlinear features of the TLD. For the latter (ii), the instantenous damping ratio gives an overview along the entire time-history, which yields a higher average damping ratio for the configuration 3(fig.11). The variation of frequency ratio ($\theta = f_{sl}/f_{str}$) is presented for damping evaluation under free

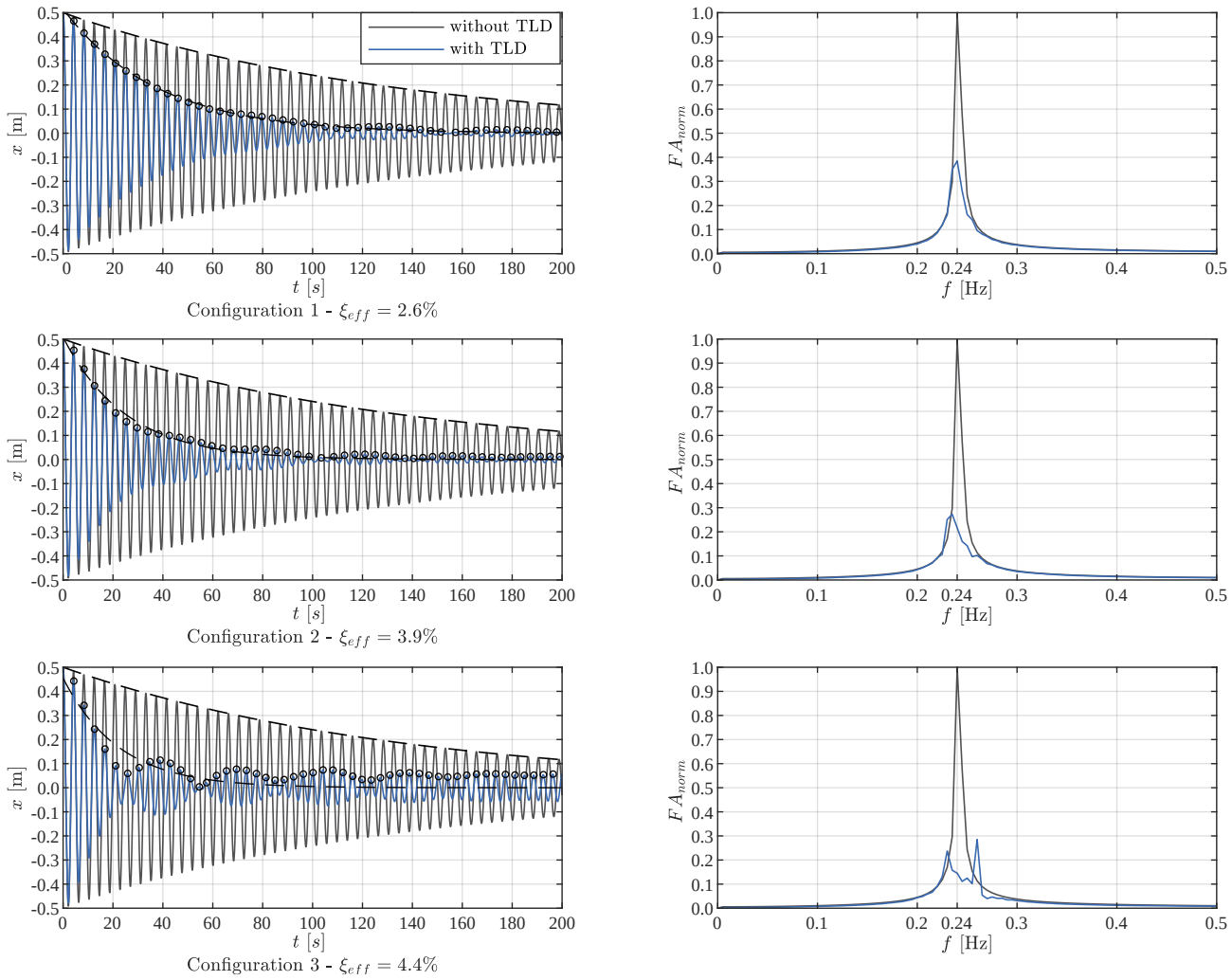

Fig. 9. Free vibration simulations for tank configurations with θ=1.

vibration tests (see fig. 10). Tank configuration 4 was selected for further study simulations, which yielded the largest effective damping with the lowest detuning if compared to configuration 3.

4.2.2. Forced-vibration

In order to understand some of the forcing features applied dynamically on a structure, forced vibration simulations are often represented by harmonic excitations. The presented cases are solved for the coupled system of equivalent SDOF structure equipped with TLD. The liquid damper with relatively high damping and fulfilling the shallow liquid depth will be further chosen for the analysis. Three sinusoidal forces were applied to the coupled system by changing the ratio of the excitation frequency (f_e) to the structural frequency (f_s). The forced vibration tests are performed under an excitation range of 0.95, 1, and 1.05 of the first frequency of the structure (see Table 3). The beating phenomenon can be observed since the spectrum frequency in fig. 12 shows the two peak frequencies relatively close. Their difference is represented by a minor frequency translated to long periods - as it can be observed on the time-history in fig. 12 - left. However, when the forcing frequency is equal to the frequency of the structure, the displacement reduction is noticeable, which is not the case otherwise. In that case, there is no displacement reduction by employing a liquid damper. An estimation of the TLD efficiency resides in the sloshing forces being out-of-phase with the input forces acting on the structure. The phase angle can be associated with damping for forced vibration simulation, and it

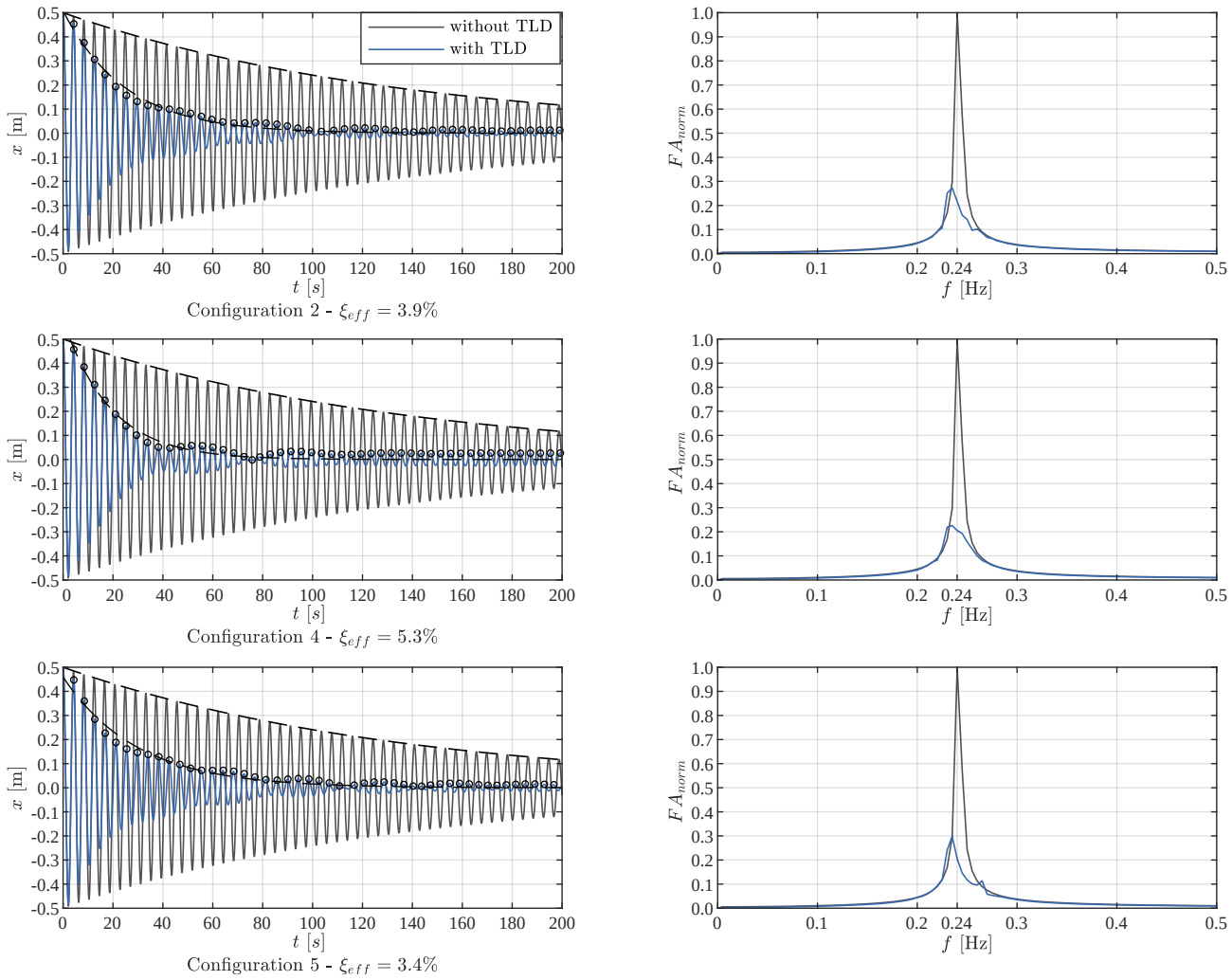

Fig. 10. Free vibration simulations for tank configurations with varying θ.

Max. Displacement [m]	No TLD [m]	TLD [m]	Reduction [%]	ϕ[°]
Case 1 (Ω=0.95)	0.081	0.094	-16	-92.0
Case 2 (Ω=1)	0.471	0.043	91	-165.0
Case 3 (Ω =1.05)	0.081	0.045	44	82.3

Table 3: Forced vibration simulation for three cases of harmonic excitation, with a force amplitude of 4 kN, $\Omega = f_e/f_{str}$. TLD case associated to configuration 4 in Table 2. Negative reduction means displacement response increase by employing TLD. The reduction is referred to the structural response with TLD compared to the case without TLD.

can be obtained from the difference between the input forcing and the response force. In order to determine the phase angle between forces, the calculation of lag time is checked by the cross-correlation between two force time histories. In fig. 12, the resonant case ($\Omega = 1$) is given by case 2, where the displacement associated with the harmonic exhibits a divergent response. By placing the TLD, this divergent response is reduced. In order to investigate the trend among the cases, the harmonic input forces are compared with the sloshing forces. In ideal cases, by employing TLD, the sloshing force would need to be in a phase of 180 degrees with the applied harmonic. In fig. 14 is shown the TLD performance for the resonance case, whereas more peculiar are the fig. 13, fig. 15, in which the phase angle changes, a reason being the nonlinear behavior of liquid motion.

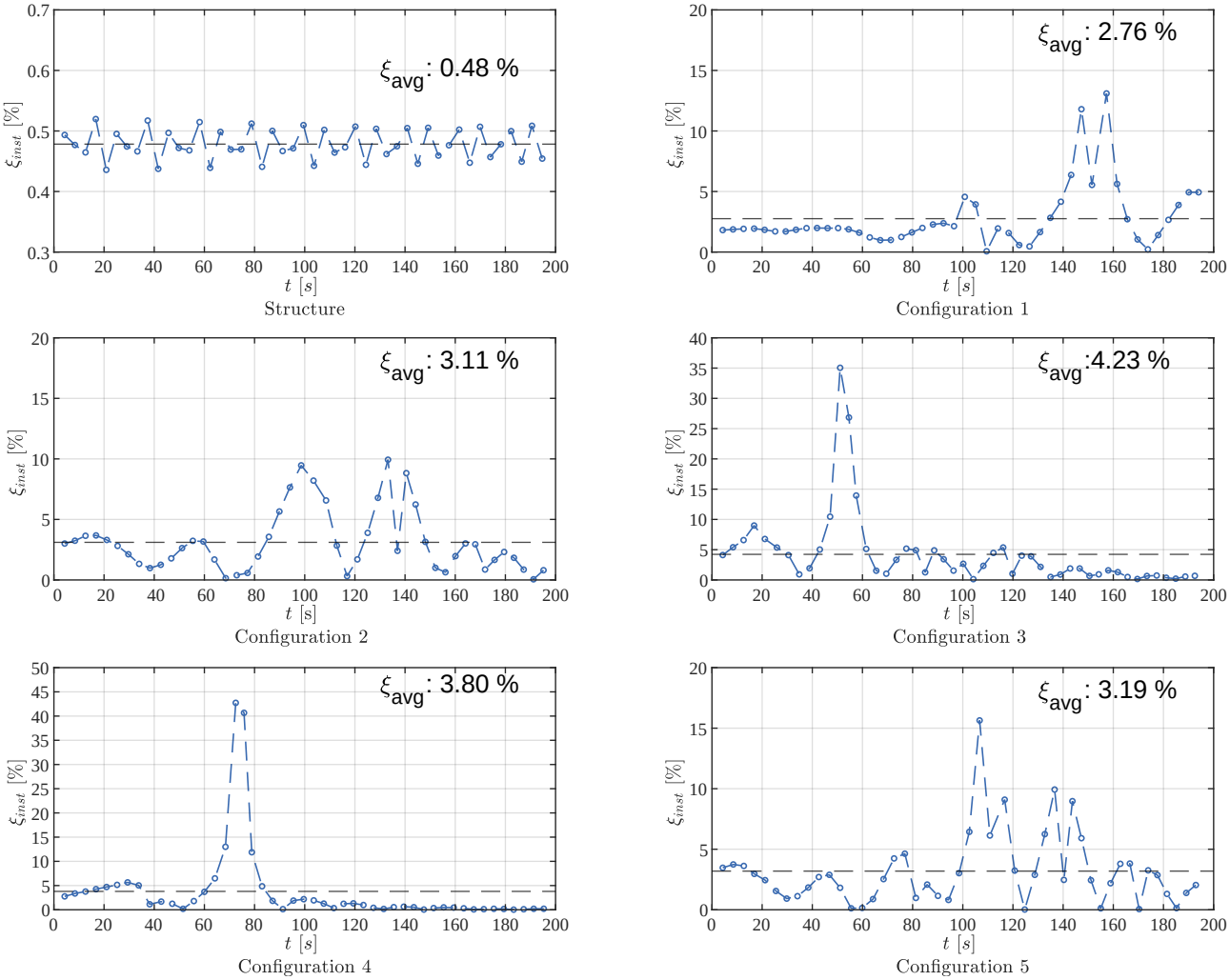

Fig. 11. Instantaneous damping ratios as a result of free vibration decays of the structure, without, and with 5 configurations of equipped TLD.

To further explore the nonlinear behavior of the liquid damper in the resonance region, the sloshing forces under harmonic excitation with different amplitudes are shown (see fig. 16). The spectrum content shows two fundamental amplitudes corresponding to the first mode ($\hat{x_1}$), and the second mode ($\hat{x_2}$). The development of secondary waves to which other modes can be excited in case of structures are being activated by higher vibration modes. Since sloshing is amplitude-dependent, higher harmonics can be activated, which can be beneficial in dissipating the energy caused by higher structural vibration modes (see fig. 17). However, this article examined only the first mode of vibration; therefore, the focus is mainly on the first sloshing frequency and its characteristics.

An equivalent TMD is proposed to compare against TLD for forced vibration cases. For this study, based on the number of iterations (10) and the swarm particles (50), the best values are found to determine the local and global optimum (see fig. 18). The TMD characteristics are further used in the wind analyses for performance comparison between TLD and TMD.

4.3. Wind-induced response

Two types of wind analyses are performed to evaluate the efficacy of the presented methodology. Firstly, vortex-induced vibration analysis is performed, allowing to analyze the response, given a narrower frequency band for the excitation force. Secondly, the buffeting response is analyzed for a 10-minute turbulent wind excitation.

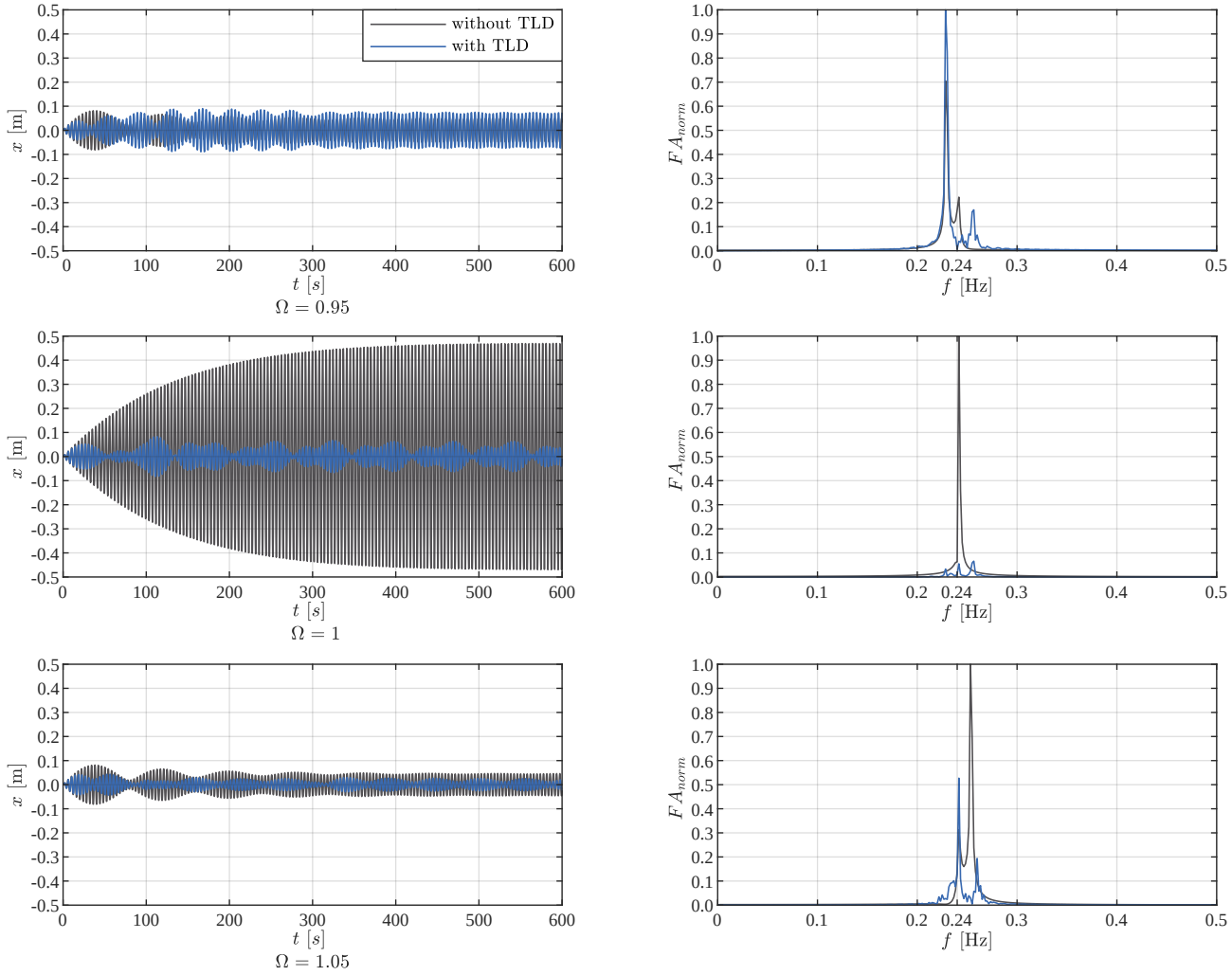

Fig. 12. Displacement responses under harmonic load with an amplitude input force of 4 kN.

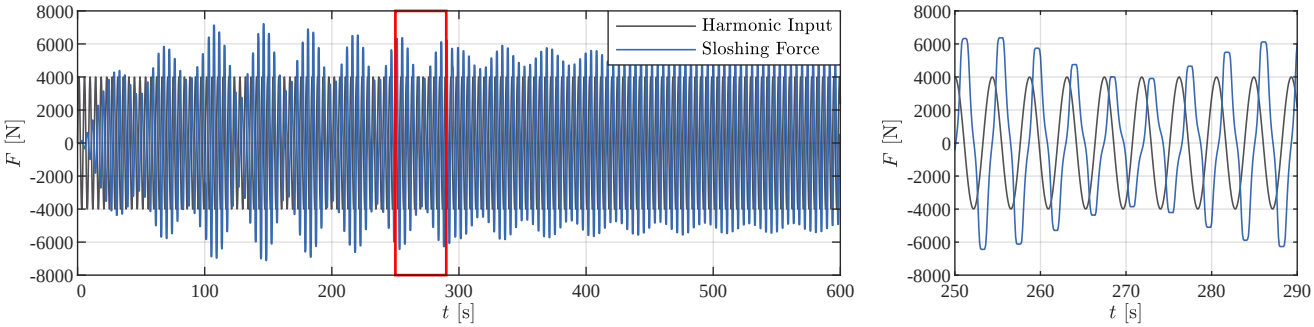

Fig. 13. External harmonic, and sloshing forces for case 1 ; time-window: ϕ = -92° (ϕ_{rad}=-1.59 rad).

4.3.1. Vortex-induced vibrations

The displacement time-history comparison with the selected TLD and the TMD are shown in fig. 19. It is well-known that the structure with low mass and low damping can feed the vortex dynamics and the energy transfer to the structure for higher amplitude displacements [51]. By investigating the resonance behavior of an equivalent

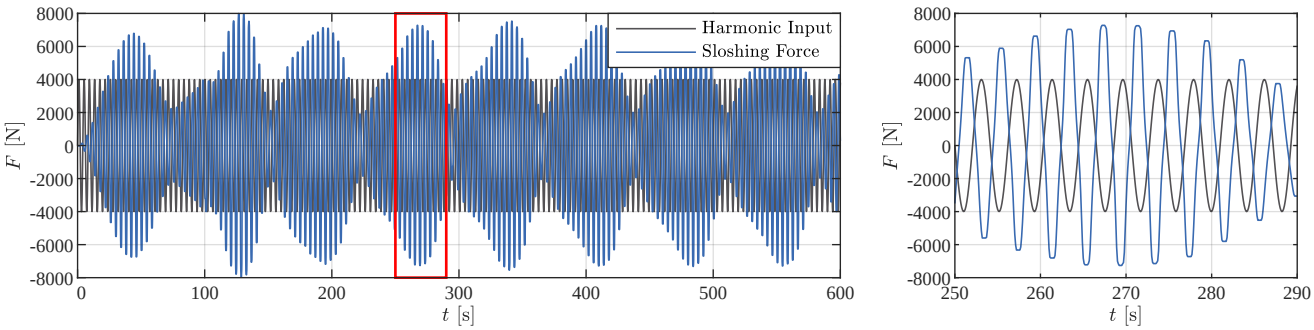

Fig. 14. External harmonic, and sloshing forces for case 2 ; time-window - ϕ = -165° (ϕ_{rad}=-2.89 rad).

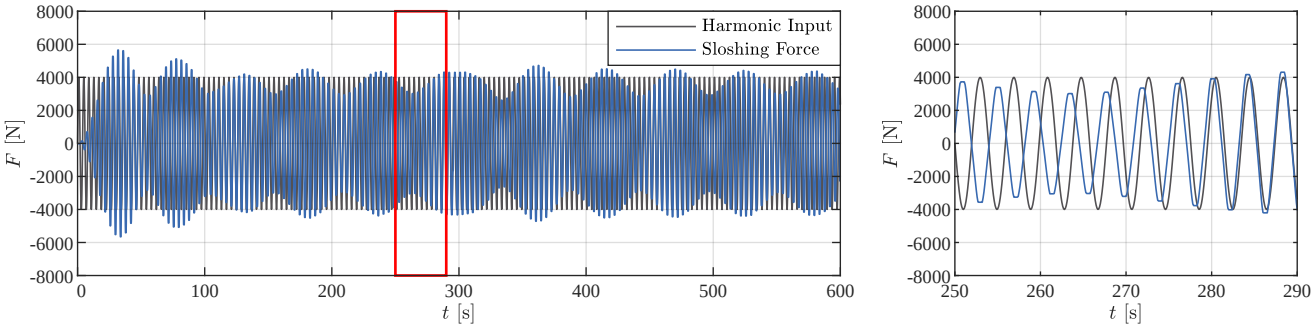

Fig. 15. External harmonic, and sloshing forces for case 3 ; time-window - ϕ = 82.3° (ϕ_{rad}=1.44 rad).

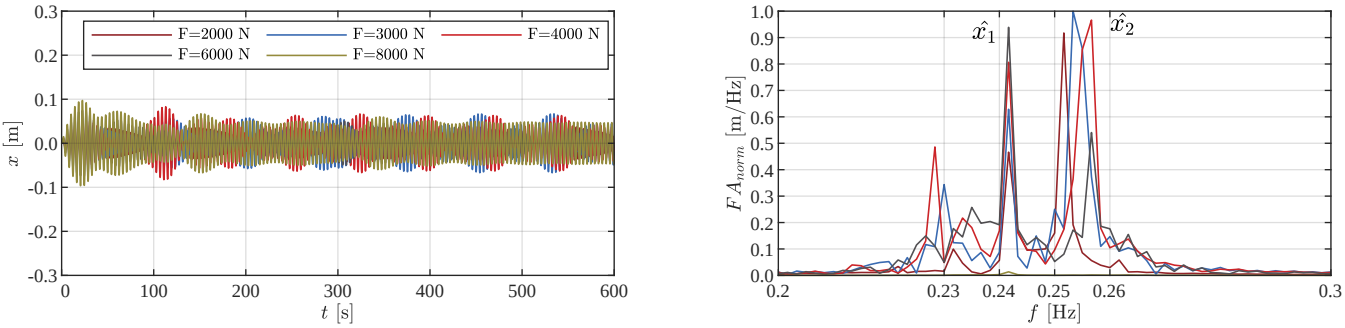

Fig. 16. Displacement response for resonance effect under different excitation force amplitudes, Ω = 1.

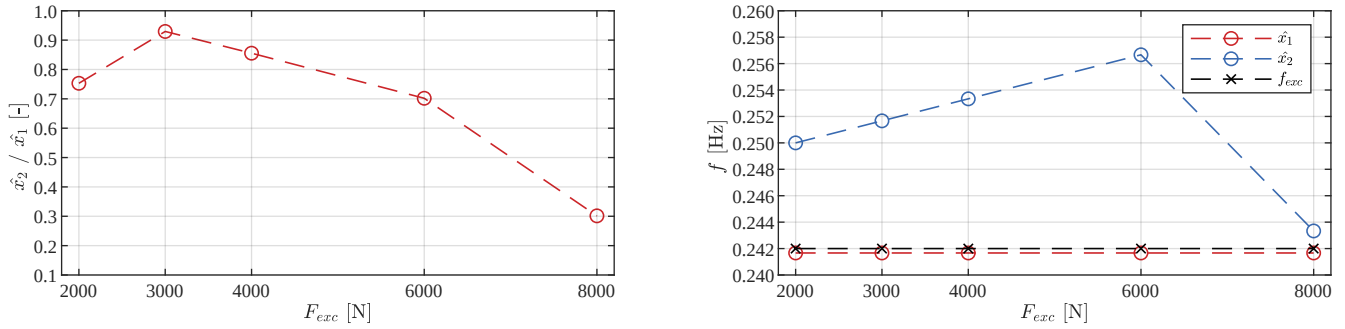

Fig. 17. Force amplitude influence on the vibration excitation of structure equipped with TLD under resonance effect, for the TLD configuration 4.

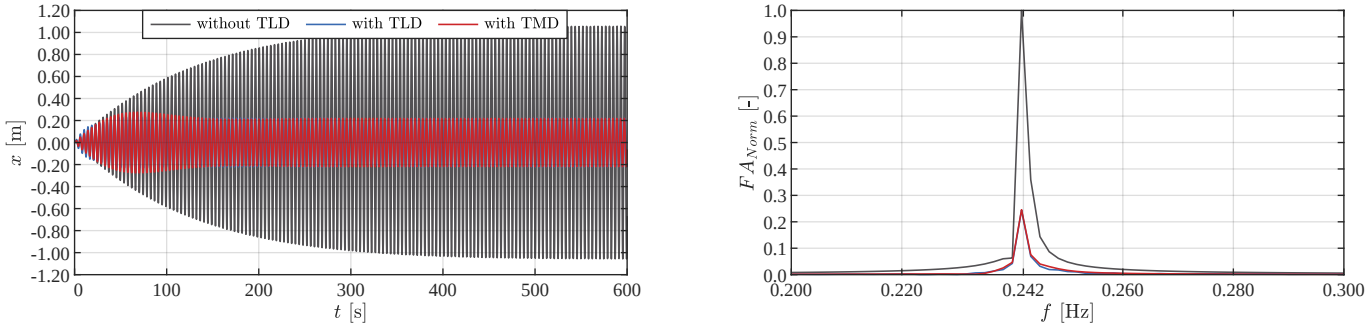

Fig. 18. Displacement response for TLD and equivalent TMD, under forced vibration applied at the tip of the chimney with a frequency equal to frequency of structure (0.242 Hz), and amplitude of force 9kN. TMD characteristics: m_{TMD} = 585 kg, ξ_{TMD} = 2.03 %, μ = 0.16 %.

Case	Peak [m]	Reduction [%]	RMS [m]
Structure	1.06	-	0.63
Structure + TMD	0.22	79	0.15
Structure + TLD	0.22	79	0.15

Table 4: Displacement response due to harmonic force applied at the tip of the chimney. Table measurements are accounted for the steady-state region [300s - 600s] (fig. 18).

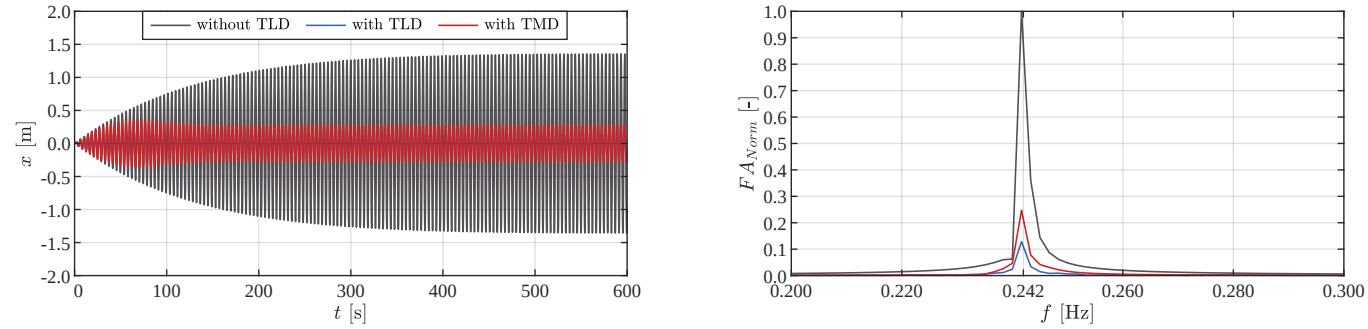

Fig. 19. Displacement tip response of the forces accounting for vortex-induced vibrations according to Eq. 18. Input parameters for cross-wind calculation according to EC1-4: K_w=0.09, K=0.13, L_c=6.32 m, y_{max}=0.43 m, St=0.18, Sc=1.37.

shedding force, the displacements for TLD and TMD show around 90% of reduction response, indicating the relative efficiency of these two passive dampers (see Table 5).

Case	Peak [m]	Reduction [%]	RMS [m]
Structure	1.36	-	0.81
Structure + TMD	0.35	74	0.20
Structure + TLD	0.17	88	0.10

Table 5: Displacement response at the tip of the chimney due to vortex shedding forces according to EC1:1-4 (fig. 19).

4.3.2. Buffeting analysis

The wind properties considered for the buffeting analysis are U= 30 m/s (at 10m height) with turbulence intensity of 20%, and terrain roughness z_0= 0.03 m (see fig. 2). The wind time-histories are simulated as described in fig. 2. A set of six 10-min time histories were analyzed for the cases of structure with TLD, with TMD, and without passive

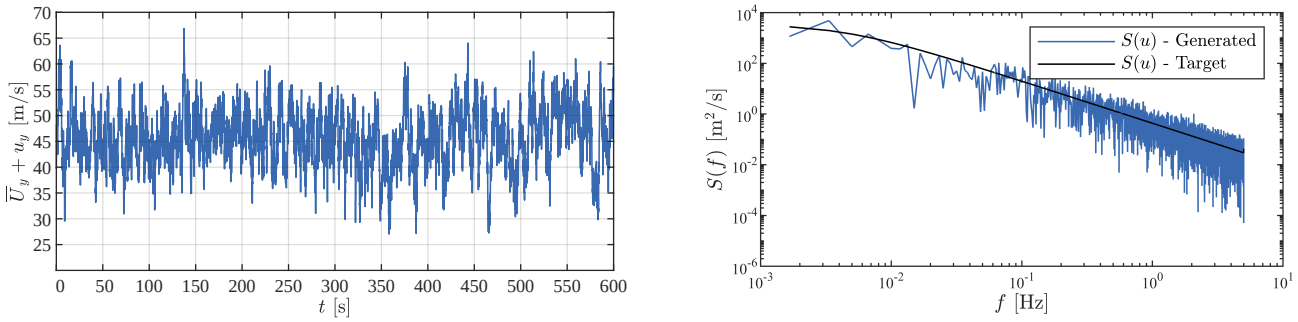

Fig. 20. Left: Time-history for 10 minutes mean and fluctuating wind speed at the tip of the chimney, based on the characteristics of fig. 2. Right: von Karman turbulence spectra based on the turbulence characteristics shown in fig. 2.

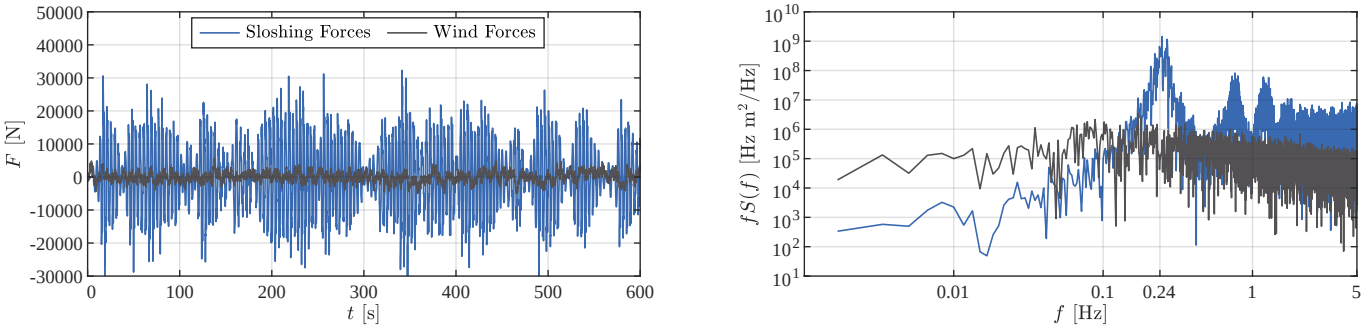

Fig. 21. Response forces due to buffeting analysis. The wind forces are subtracted from the mean response. Right: The spectrum content of the force response components in logarithmic scale. Buffeting response at the tip of the chimney. TLD Characteristics (L=6.4 m, h_w=0.945 m, m_{tld}=6048 kg), μ=1.7 %.

dampers, respectively. An example of a simulated time history is given in fig. 20, with the corresponding spectrum. The wind forces acting on the structure are smaller than the sloshing forces (see fig. 21 - left). However, wind loading exhibits a wide range of frequency components, unlike harmonic force targeted to a specific frequency. To examine the characteristic features of both sloshing and wind forces, respectively, the power spectral density is shown in fig. 21 - right. The generated wind forces show a low-frequency range, with higher energy contribution for frequencies lower than the first structural frequency. On the other hand, the sloshing forces, as a result of wind excitation, display a higher energy content around the sloshing frequency, thus targeting the structural vibration mode. It can be seen that the normalized frequency peak is slightly shifted to the right of the structural frequency. This can be attributed to higher sloshing modes that may also be symmetric. However, the TLD was tuned to the first antisymmetric sloshing mode. The nonlinearities arising in the fluid-structure interaction of the TLD are probably the reason for the frequency shift, i.e., the departure of the linear sloshing frequency.

The effectiveness of the TLD under random wind excitation is shown in terms of displacement response at the tip of the chimney (see fig. 22). The time-domain analysis shows that among the 10-minutes interval, there are time windows in which there is a noticeable decrease in displacement amplitude. The plot shows the dynamic displacements around the deflected position due to mean wind. From the normalized power spectral density, one can distinguish the attenuation response for the first vibration mode. In fig.24, absolute peak and RMS responses of the chimney tip are shown based on six seeds of 10-min wind simulations.

Table 6 shows the average of peak and RMS for three scenarios: no damper, TMD, and TLD. The effective TMD and TLD yield similar results. However, given the randomness of the buffeting loading, the TLD or the TMD cannot be activated quickly for optimal reduction. Unlike VIV, the broad bandwidth of frequencies for buffeting response allows specific time windows of displacement reduction (see fig. 21). The TMD is compared with the chosen configuration from the above section. On the one hand, this indicates the efficacy and the simplicity of using an equivalent TMD

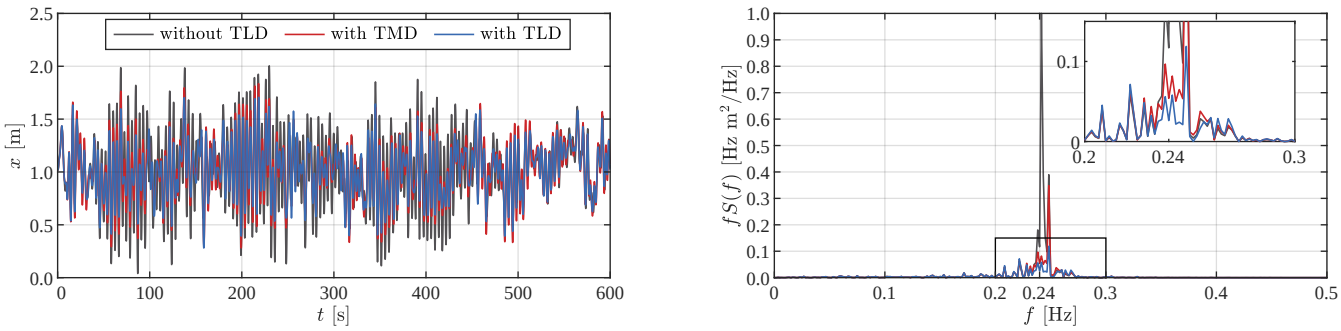

Fig. 22. Buffeting response at the tip of the chimney. TLD Characteristics (L=6.4 m, h_w=0.945 m, m_{tld}=6048 kg), μ=1.7 %. TMD characteristics: m_{TMD} = 585 kg, ξ_{TMD} = 2.03 %, μ = 0.16 %.

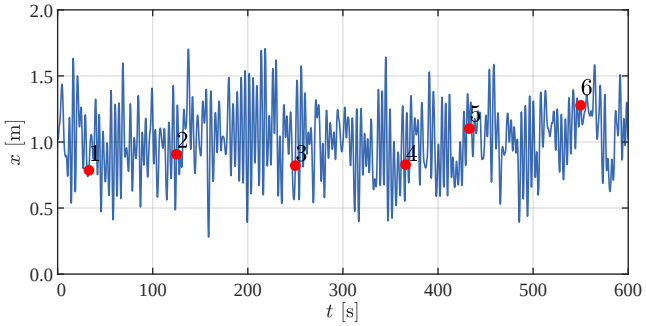

Fig. 23. Buffeting response at the tip of the chimney, equipped with TLD.

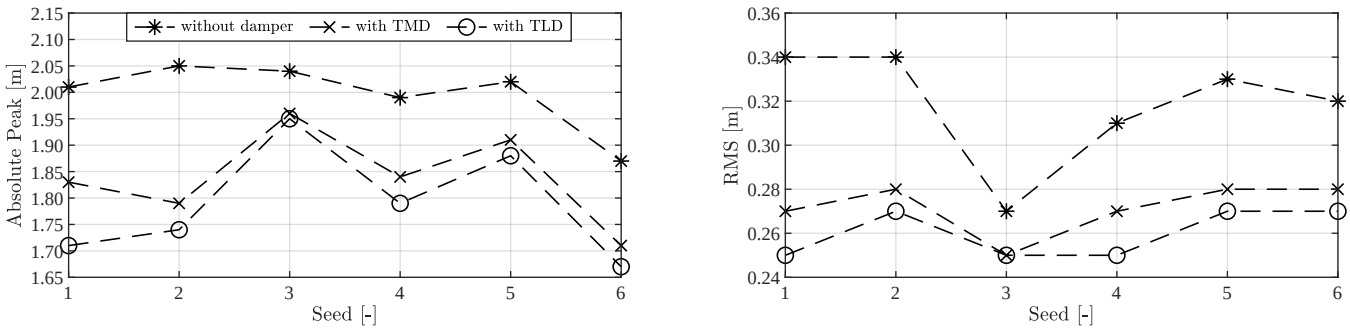

Fig. 24. Left: Absolute peak displacements at the tip of the chimney for the structure (i) with no control system, (ii) with TMD, and (iii) with TLD, following the six sets of 10 minutes mean and fluctuating wind speed. Right:Correspondent root-mean-square displacements for similar setup conditions.

Cases [1-6]	$\overline{\text{Peak}}$ [m]	$\overline{\text{Peak}}$ reduction [%]	$\overline{\text{RMS}}$ [m]
Structure	1.99	-	0.32
Structure + TMD	1.84	7.85	0.27
Structure + TLD	1.79	10.29	0.26

Table 6: Deterministic averaged results for buffeting analyses, for six 10-minutes wind simulations. RMS is calculated by subtracting the mean response. The percentage column shows the reduction by employing the passive dampers to the structure.

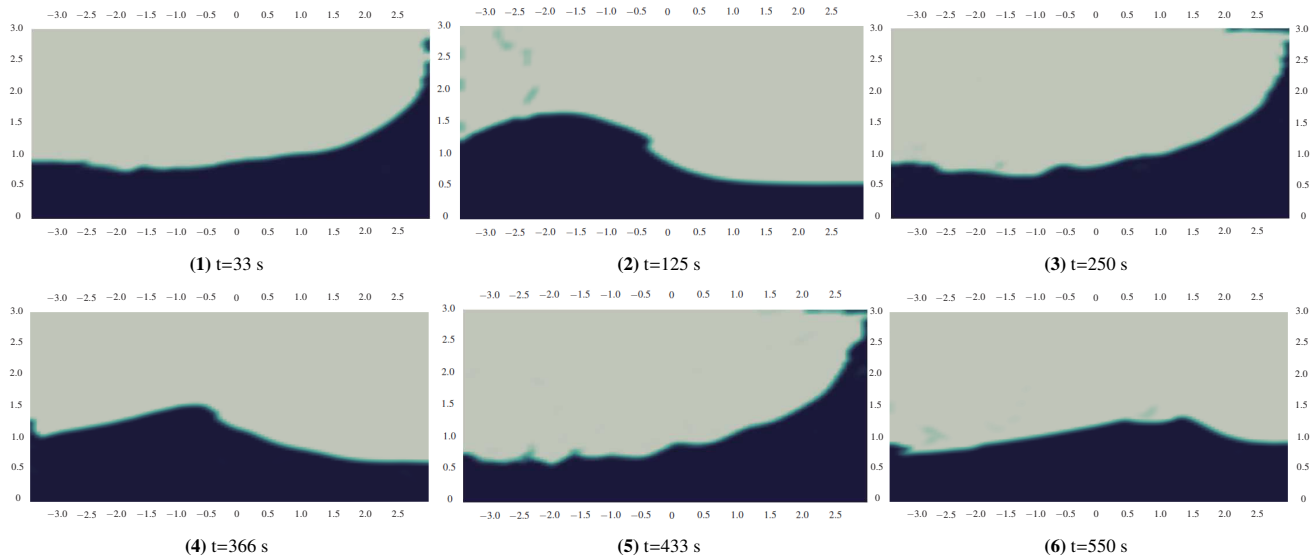

(1) t=33 s **(2)** t=125 s **(3)** t=250 s

(4) t=366 s **(5)** t=433 s **(6)** t=550 s

Fig. 25. Time-instant snapshots for liquid damper under buffeting analysis.

model instead of TLD. On the other hand, the TLD exhibits nonlinear features, to which the linear TMD is limited unless higher reduced-order models are used. For this study case, only the first vibration mode was targeted and analyzed to prove the efficiency of the coupling method with TLD. In fig. 23 is shown the response time-history of the structure, while fig. 25 depicts the corresponding snapshots of the TLD at the indicated locations.

5. Application: Human Comfort Analysis of a High-Rise Building

5.1. Reference Structure

A tall building with constant cross-section along the height is showcased for the habitability comfort assessment using the partitioned numerical coupling (Aerodynamic Model - Structural Model - Sloshing Model). The along-wind response acceleration is investigated and evaluated according to well-established standards [52, 53, 54], since users' comfort in perceiving motion is a criterion evaluated by story acceleration. Tamura et. al [55] have shown the probabilistic perception of thresholds based on AIJ-RJB guidelines. Because perception motion has a subjective character, the evaluation criteria have been described through several curves describing the percentage of people to perceive the vibrations (i.e., H90 - 90% of people with perceived vibrations). As per [55], the peak acceleration is adopted for simplicity, being understood easily by building owners or designers for motion perception, whereas root-mean-square (RMS) could be more appropriate for the physical parameter for the habitability evaluation in terms of long term tolerance.

The structural model of the high-rise building is discretized in finite elements according to the dynamic structural characteristics, along a height of 383 meters, corresponding to the first mode of translation [56]: M_1 = 52596 t, f_1 = 0.1425 Hz, ξ_1 = 0.02 , K_1 = 42250 kN/m. The objective is to reduce the acceleration response below the thresholds of motion perception levels. In order to test the efficiency of using TLDs to dissipate energy, the sloshing dampers are primarily targeted to the predominant frequency, where the significant mass of the structure is activated under external excitation. The Tuned Mass Damper (TMD) characteristics of a tall building [57] have been selected as the supplemental damper, which are used in the comparative analyses with sloshing dampers.

5.2. TLD Predesign

The analytical method from eq. (16) provides an evaluation of the sloshing frequency expressed through the following parameters: height of water (h_w) and the length of the container (L) (see eq. (16)). Following the shallow water criterion, the frequency of sloshing is chosen to be approximately equal to the frequency of the structure (θ =

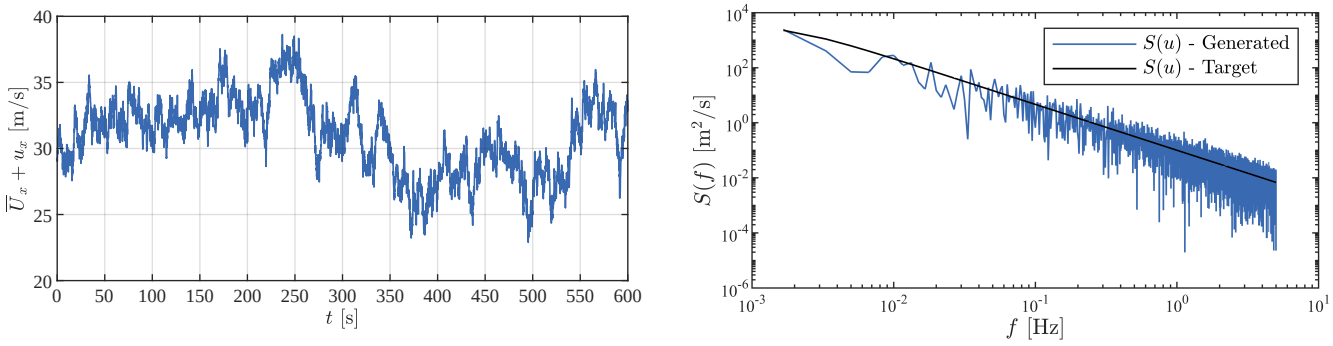

Fig. 26. Left: Time-history for 10 minutes mean and fluctuating wind speed at the top of the structure. Right: Von Karman turbulence spectra.

$f_{sl}/f_{str} \lesssim 1$). Two other cases are presented in which the sloshing frequency is taken as a lower ratio of the structural frequency.

For this purpose, three tank geometry cases have been chosen to compare the acceleration response at the top of the building. Based on this comparison criteria, the TLD with the most effective amplitude reduction is chosen for further investigation. Furthermore, since the mass of one TLD is significantly small compared with the TMD mass, several TLD setups are used with the chosen configuration, namely, (i) 1 TLD, (ii) 2 similar TLDs at the top level, and (iii) 4 similar TLDs (2 TLDs placed at the top level and 2 TLDs at one level below).

Tall Building TLD Case	L [m]	h_w [m]	f_{sl} [Hz]	θ (f_{sl}/f_{str}) [-]	Peak [m]	[%]	RMS [m]	[%]
Configuration 1	14.70	1.99	0.146	1.03	0.166	0.07	0.061	4.81
Configuration 2	15.45	2.00	0.139	0.98	0.153	7.81	0.056	11.62
Configuration 3	15.95	2.00	0.135	0.95	0.143	13.67	0.053	16.62

Table 7: Deterministic results for buffeting analyses for similar input characteristics of 10-minutes wind conditions. The percentage columns after peak and RMS accelerations show the reductions compared to the structure's acceleration response without a damper.

5.3. Buffeting Analyses

Based on the preliminary studies from table 7, configuration 3 has been chosen for testing the TLD with three different setups explained in the previous section. As a reference for the structural response equipped with a supplemental damper, the present configuration of TMD is taken for comparisons (m_{TMD} = 660 t, f_d = 0.1404 Hz, ξ_{TMD} = 0.131 [57]).

The wind characteristics for the buffeting analysis have the following properties with an incoming wind speed U= 19 m/s (at 10m height) and turbulence intensity of 20%, terrain roughness (z=0.03 m), and turbulence length scale (L_x=340 m), for a scenario of one-year recurrent interval. A set of six 10-min time histories were analyzed for the cases of structure with TLD, with TMD, and without passive dampers, respectively. An example of a simulated time history is given in fig. 26, with the corresponding spectrum. The acceleration responses are presented in fig. 28 - left side.

In order to determine the drag coefficient for the outer cross-section shape of the structure, a CFD static simulation was performed using a validated CFD software based on Vortex-Particle Method [58],[59]. The average drag coefficient ($\overline{C_D}$ = 1.4) was used in the aerodynamic force calculation (eq. (3)) for the buffeting analyses.

To examine the characteristic features of both sloshing and wind forces, respectively, the power spectral density is shown in fig. 27 - right. The generated wind forces show a low-frequency range, with higher energy contribution for frequencies lower than the first structural frequency. On the other hand, the sloshing forces resulting from wind excitation display a higher energy content around the sloshing frequency, thus targeting the structural vibration mode.

The effectiveness of the TLD under random wind excitation is shown in terms of acceleration response at the top of the structure (see fig. 29). The time-domain analysis (S3) shows that among the 10-minute interval, there are

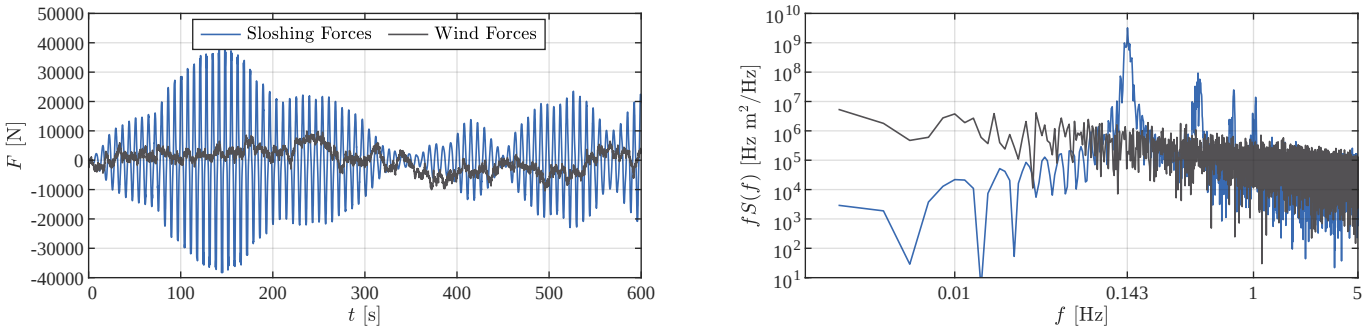

Fig. 27. Left: Response forces due to buffeting analysis, at the top node, equipped with 1 TLD. The wind forces are subtracted from the mean response. Right: The spectrum content of the force response components in logarithmic scale.

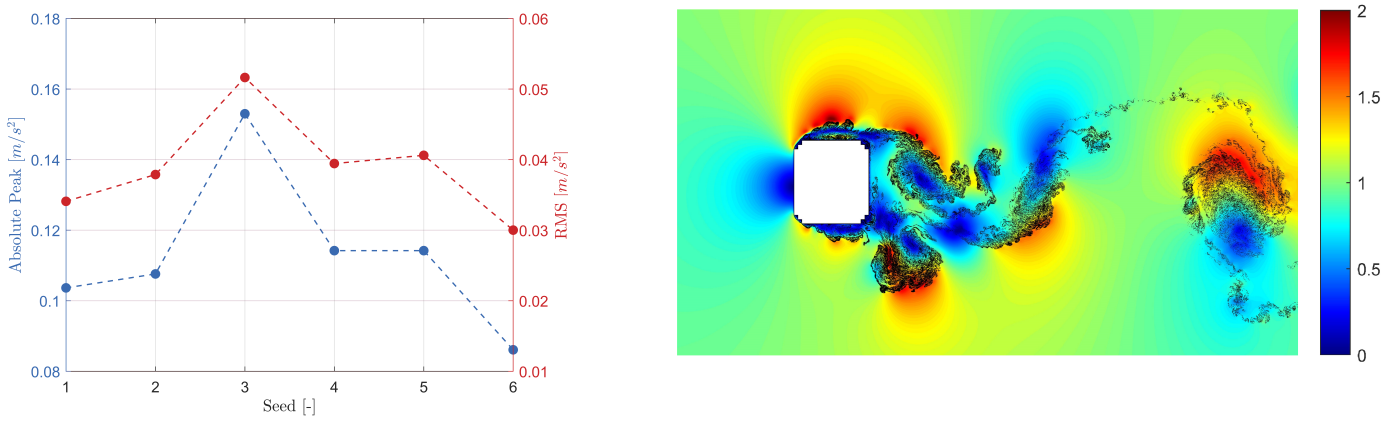

Fig. 28. Left: Absolute peak and root-mean-square accelerations at the top of the structure, following the six sets of 10 minutes mean and fluctuating wind speed. Right: Time-instant of an iso-velocity contour of the flow past bluff section. The contour legend shows the normalized wind speed values with respect to the incoming wind flow.

time windows in which there is a noticeable decrease in acceleration amplitude. From the normalized power spectral density, one can distinguish the attenuation response for the first vibration mode.

Table 8 shows the acceleration peak and RMS for five scenarios: no damper, TMD, 1 TLD, 2 TLDs mounted at the same level, and 4 TLDs (two mounted at the top level and two mounted at a lower level), respectively. The effective TMD and TLD yield similar results. Given the randomness of the buffeting loading, the TLD or the TMD cannot be activated quickly for optimal reduction.

Acceleration Tip Response	Str	Str + TMD	Str + 1 TLD	Str + 2 TLDs	Str + 4 TLDs
Mass ratio ($\mu = m_{damper} / m_{str}$) [%]	-	1.250	0.061	0.122	0.244
Absolute Peak [m/s^2]	0.153	0.086	0.122	0.107	0.113
Peak reduction [%]	-	43.66	19.83	29.96	26.04
RMS [m/s^2]	0.052	0.026	0.042	0.038	0.037
RMS reduction [%]	-	49.50	17.75	25.65	28.14

Table 8: Deterministic results for buffeting analyses for 10-minutes average wind speed simulations. The percentage column for both peak and RMS accelerations shows a reduction in comparison with the acceleration response of the structure without a damper—wind speed 19m/s, with turbulence intensity 20%.

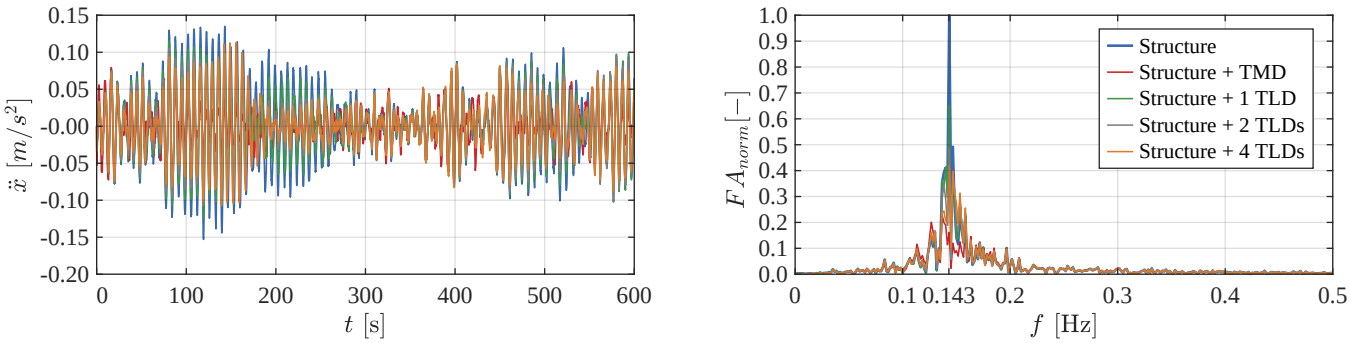

Fig. 29. Left: Time-history (Seed 3) acceleration response at the top of the structure for multiple scenarios. Right: The associated spectrum content of the acceleration response. TLD Characteristics of one tank (L=15.95 m, h_w=2 m, m_{tld}=31900 kg).

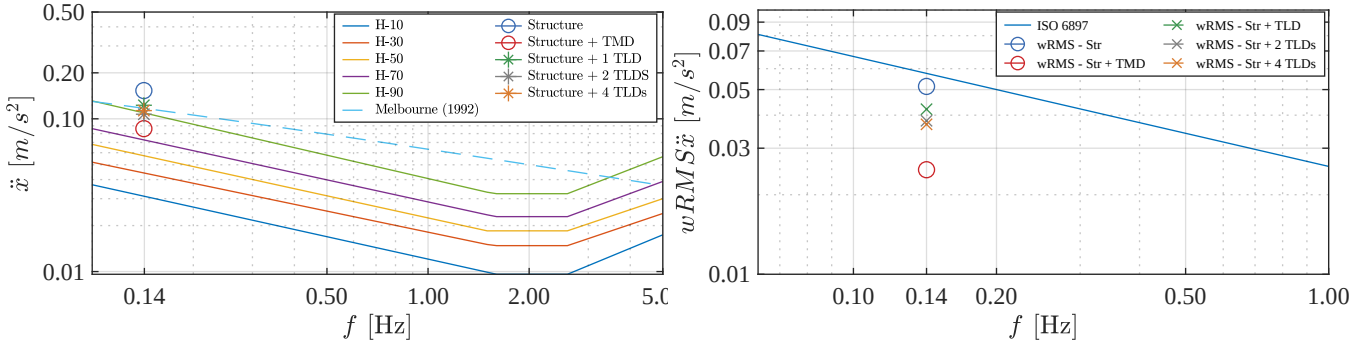

Fig. 30. Left: Evaluation curves for human comfort according to AIJ-RIB (2004) and Melbourne [60], corresponding to one-year recurrency interval. The peak accelerations for the structural response at the top story due to wind are represented as deterministic values based on seeded (S3) 10-min average wind time-history. Right: The weighted RMS acceleration value is calculated according to ISO 2631 [53].

5.4. Comfort Criteria Assessment

Habitability criteria is a subjective assessment; however, the evaluation can be classified in design level criteria based on peak acceleration response [55] and RMS response [52]. Following the buffeting analysis (#3) results obtained in fig. 29, and its corresponding values from table 8, results are plotted with the respective evaluation curves in fig. 30. Regarding the peak acceleration values, the structure response is above the criterion level (Melbourne and H-90). In contrast, the cases for the structure with TMD, and 2 TLDs, respectively, are within the threshold limit provided by Melbourne and H-90. However, in the structure equipped with 4 TLDs, the criterion is met only for the Melbourne curve, above the H-90 threshold. For the weighted RMS values, all the scenario values are within the limit imposed by ISO 6897.

6. Conclusions

In this article, a numerical coupling method for fluid-structure-interaction was proposed between (i) structural model, (ii) aerodynamic model, and (iii) CFD sloshing model. The purpose of the study was to present a novel framework that embeds the three models in a partitioned approach, with the highlight on efficiency of TLD under broad-band frequencies, and narrow-band frequency responses. The structural model consisted of solving the equation of motion numerically, given the input properties, i.e., mass, damping, and stiffness. The properties were selected for structures with dynamic characteristics represented by the first vibration mode. The forcing terms were composed of linear force addition between two components: (i) the aerodynamic model and (ii) CFD sloshing model. The aerodynamic model was comprised of either buffeting quasi-steady aerodynamic force model or the VIV model. The CFD model for sloshing force was based on VOF, a mesh grid method, wherein a phase-fraction interface between the two liquids, water, and air, was considered for the fluid pressure calculation to determine the sloshing force.

The CFD sloshing model has shown good results in comparison with the forces generated under the same harmonic excitation in a shaking-table experiment. Further on, an application of the framework to the chimney and an application to a high-rise building were presented. Herein, the predesign of the TLD, an equivalent TMD model, buffeting analysis based on simulated free-stream turbulence, and VIV analysis were studied. Six seeds of 10-minute wind were evaluated for buffeting analyses with a corresponding average value. It was shown that for buffeting analyses, the peak displacement response was reduced in average by 10.29% when the TLD was equipped at the tip of the chimney. Similarly, the equivalent TMD model has shown an average reduction of 7.85%. For the VIV analysis, an approach based on the European wind design code was presented for calculating the cross-wind amplitudes, in which an equivalent VIV force was applied along a correlation length specific to the first mode of vibration of the chimney. The peak displacement response was reduced up to 88 % by using TLD and 74% with an equivalent TMD. These results show that for resonance type phenomenon, with narrow bandwidth, the dampers were more effective in reducing the peak displacements.

Habitability criteria were assessed for peak accelerations and RMS values using multiple scenarios of TLDs. It was shown that for buffeting analysis, the peak acceleration response was reduced with: (i) 19.83% when the TLD was equipped at the top of the building, (ii), 29.96% when 2 TLDs were equipped at the top, and (iii) 26.04% when 4 TLDs are equipped (2 at the top level and 2 at the level below) . Similarly, the TMD model has shown a reduction of 43.66%. The RMS values for the scenarios mentioned above show a similar trend, mentioning that the RMS for the structure equipped with 4 TLDs is lower than the structure with 2 TLDs. These results show that for the buffeting type phenomenon, by varying the scenarios of liquid dampers, there is a reduction difference, but with no more than 11% for the studied cases (1 TLD, 2 TLDs, and 4 TLDs, respectively). Although the acceleration reduction for the structure equipped with the TLD scenarios is overall lower than the structure with TMD, the mass of 4 TLDs is approximately five times lower than the mass of TMD. The latter shows that the TLD can provide a good alternative for supplemental dampers while reducing the mass significantly.

The methodology of using the VOF model for a TLD has shown a reliable alternative to experiments for both TLD predesign and analysis. The VOF model can capture nonlinear forces and provide realistic modeling of the TLD, which otherwise is intractable by semi-analytical models. The TLDs can significantly reduce the wind-induced response of structures that is critical for serviceability limit states and fatigue limit.

The numerical coupling framework offers the possibility of evaluating a structure equipped with TLD system under various excitations. In this way, a cost-efficient manner to ensure the reliability of the TLD design can be assessed for the structural design analyses. It represents a high-fidelity design analysis for structures equipped with TLD under hazard actions. The versatility of the coupled model consists of analyzing various structures, under the information of dynamic properties. Moreover, in case of change of dynamic properties, by monitoring instrumentation, a re-design of TLD can be investigated by numerical coupled analyses at rather reduced computational time. Multiple TLDs can be shown to achieve higher response reduction in the buffeting analysis and target higher modes of vibration to which additional damping might be considered. The limitation of the current partitioned numerical approach is represented by the two-dimensional TLD use in structural response as a result of uni-directional excitation, with disregard of in-plane interaction such as torsional motion, or influence of higher modes of vibration. The possibility of using multi-modes can be applied to the existing coupling framework, with a more in-depth study of the nonlinear and amplitude dependent forces. With the new coupling framework, TLD behavior for comparison studies can be considered with other CFD models or with reduced-order models.

7. Acknowledgement

The research support was partially provided through a scholarship from German State of Thuringia [Thüringer Graduiertenförderung]. The author is also thankful for the support of the Geotechnical Department within Bauhaus-University Weimar in conducting the experiments at the shaking table.

References

[1] K. Y. Billah, R. H. Scanlan, Resonance, tacoma narrows bridge failure, and undergraduate physics textbooks, American Journal of Physics 59 (1991) 118–124.

[2] T. Abbas, I. Kavrakov, G. Morgenthal, Methods for flutter stability analysis of long-span bridges: a review, Proceedings of the Institution of Civil Engineers - Bridge Engineering 170 (2017) 271–310.
[3] K. Kwok, B. Samali, Performance of tuned mass dampers under wind loads, Engineering Structures 17 (1995) 655–667.
[4] R. Rana, T. T. Soong, Parametric study and simplified design of tuned mass dampers, Engineering Structures 20 (1998) 193–204.
[5] G. W. Housner, The dynamic behavior of water tanks, Bulletin of the Seismological Society of America 53(2) (1963) 381–387.
[6] M. Ifrim, C. Bratu, The effect of seismic action on the dynamic behaviour of elevated water tanks, Proceedings of the 4th World Conference on Earthquake Engineering, Santiago 3(B-4) (1969) 127–142.
[7] A. Kareem, Reduction of wind induced motion utilizing a tuned sloshing damper, Journal of Wind Engineering and Industrial Aerodynamics 36 (1990) 725–737.
[8] T. Wakahara, T. Ohyama, K. Fujii, Suppression of wind-induced vibration of a tall building using tuned liquid damper, Journal of Wind Engineering and Industrial Aerodynamics 43 (1992) 1895–1906.
[9] Y. Tamura, R. Kousaka, V. J. Modi, Practical application of nutation damper for suppressing wind-induced vibrations of airport towers, Journal of Wind Engineering and Industrial Aerodynamics 43 (1992) 1919–1930.
[10] Z. Wang, F. Ubertini, S. Laflamme, Ensemble of long short-term memory recurrent neural network for semi-active control of tuned liquid wall damper, Engineering Structures 270 (2022) 114771.
[11] N. Cavalagli, A. Agresta, C. Biscarini, F. Ubertini, S. Ubertini, Enhanced energy dissipation through 3d printed bottom geometry in tuned sloshing dampers, Journal of Fluids and Structures 106 (2021) 103377.
[12] O. M. Faltinsen, A. N. Timokha, Sloshing, Cambridge University Press, Cambridge, 2009.
[13] R. A. Ibrahim, Liquid sloshing dynamics: Theory and applications / Raouf A. Ibrahim, Cambridge University Press, Cambridge, 2005.
[14] L. Sun, Y. Fujino, A semi-analytical model for tuned liquid damper (tld) with wave breaking, Journal of Fluids and Structures 8 (1994) 471–488.
[15] C. G. Koh, S. Mahatma, C. M. Wang, Theoretical and experimental studies on rectangular liquid dampers under arbitrary excitations, Earthquake Engineering & Structural Dynamics 23 (1994) 17–31.
[16] X. Deng, M. J. Tait, Equivalent mechanical models of tuned liquid dampers with different tank geometries, Canadian Journal of Civil Engineering 35 (2008) 1088–1101.
[17] J.-K. Yu, T. Wakahara, D. A. Reed, A non–linear numerical model of the tuned liquid damper, Earthquake Engineering & Structural Dynamics 28 (1999) 671–686.
[18] L. M. Sun, Y. Fujino, P. Chaiseri, B. M. Pacheco, The properties of tuned liquid dampers using a tmd analogy, Earthquake Engineering & Structural Dynamics 24 (1995) 967–976.
[19] B. Godderidge, S. Turnock, M. Tan, C. Earl, An investigation of multiphase cfd modelling of a lateral sloshing tank, Computers & Fluids 38 (2009) 183–193.
[20] E. Berberović, N. P. van Hinsberg, S. Jakirlić, I. V. Roisman, C. Tropea, Drop impact onto a liquid layer of finite thickness: dynamics of the cavity evolution, Physical review. E, Statistical, nonlinear, and soft matter physics 79 (2009) 036306.
[21] N. Cavalagli, C. Biscarini, A. L. Facci, F. Ubertini, S. Ubertini, Experimental and numerical analysis of energy dissipation in a sloshing absorber, Journal of Fluids and Structures 68 (2017) 466–481.
[22] H. Akyildız, N. Erdem Ünal, Sloshing in a three-dimensional rectangular tank: Numerical simulation and experimental validation, Ocean Engineering 33 (2006) 2135–2149.
[23] J. Gómez-Goñi, C. A. Garrido-Mendoza, J. L. Cercós, L. González, Two phase analysis of sloshing in a rectangular container with volume of fluid (vof) methods, Ocean Engineering 73 (2013) 208–212.
[24] S.-c. Jiang, B. Teng, W. Bai, Y. Gou, Numerical simulation of coupling effect between ship motion and liquid sloshing under wave action, Ocean Engineering 108 (2015) 140–154.
[25] A. Crespo, J. M. Domínguez, B. D. Rogers, M. Gómez-Gesteira, S. Longshaw, R. Canelas, R. Vacondio, A. Barreiro, O. García-Feal, Dualsphysics: Open-source parallel cfd solver based on smoothed particle hydrodynamics (sph), Computer Physics Communications 187 (2015) 204–216.
[26] M. D. Green, Y. Zhou, J. M. Dominguez, M. G. Gesteira, J. Peiró, Smooth particle hydrodynamics simulations of long-duration violent three-dimensional sloshing in tanks, Ocean Engineering 229 (2021) 108925.
[27] A. Marsh, M. Prakash, E. Semercigil, Ö. F. Turan, A study of sloshing absorber geometry for structural control with sph, Journal of Fluids and Structures 27 (2011) 1165–1181.
[28] D. K. Kwon, A. Kareem, Hybrid simulation of a tall building with a double–decker tuned sloshing damper system under wind loads, The Structural Design of Tall and Special Buildings (2020).
[29] R. W. Clough, J. Penzien, Dynamics of structures, Computers and Structures, Berkeley Calif., 2nd ed., rev edition, 2010.
[30] I. Kavrakov, G. Morgenthal, A synergistic study of a cfd and semi-analytical models for aeroelastic analysis of bridges in turbulent wind conditions, Journal of Fluids and Structures 82 (2018) 59–85.
[31] I. Kavrakov, A. McRobie, G. Morgenthal, Data-driven aerodynamic analysis of structures using gaussian processes, Journal of Wind Engineering and Industrial Aerodynamics 222 (2022) 104911.
[32] I. Kavrakov, G. Morgenthal, Aeroelastic analyses of bridges using a pseudo-3d vortex method and velocity-based synthetic turbulence generation, Engineering Structures 176 (2018) 825–839.
[33] I. Kavrakov, G. Morgenthal, A comparative assessment of aerodynamic models for buffeting and flutter of long-span bridges, Engineering 3 (2017) 823–838.
[34] I. Kavrakov, D. Legatiuk, K. Gürlebeck, G. Morgenthal, A categorical perspective towards aerodynamic models for aeroelastic analyses of bridge decks, Royal Society open science 6 (2019) 181848.
[35] European Committee for Standardization, Eurocode 1: Actions on structures - part 1-4: General actions - wind actions, 2010.
[36] E. Simiu, R. H. Scanlan, Wind effects on structures: An introduction to wind engineering / Emil Simiu, Robert H. Scanlan, Wiley, New York and Chichester, 2nd ed. edition, 1986.
[37] G. Solari, G. Piccardo, Probabilistic 3-d turbulence modeling for gust buffeting of structures, Probabilistic Engineering Mechanics 16 (2001)

73–86.
[38] Q. Ding, L. Zhu, H. Xiang, An efficient ergodic simulation of multivariate stochastic processes with spectral representation, Probabilistic Engineering Mechanics 26 (2011) 350–356.
[39] C. Hirt, B. Nichols, Volume of fluid (vof) method for the dynamics of free boundaries, Journal of Computational Physics 39 (1981) 201–225.
[40] J. Brackbill, D. Kothe, C. Zemach, A continuum method for modeling surface tension, Journal of Computational Physics 100 (1992) 335–354.
[41] H. G. Weller, G. Tabor, H. Jasak, C. Fureby, A tensorial approach to computational continuum mechanics using object-oriented techniques, Computers in Physics 12 (1998) 620.
[42] Sreekanth Buddhiraju, Numerical methods for Liquid Sloshing Dampers for coupling with structure dynamic analysis, Master thesis, Bauhaus University, Weimar, 2021.
[43] A. Y. T. Leung, H. Zhang, Particle swarm optimization of tuned mass dampers, Engineering Structures 31 (2009) 715–728.
[44] J. Kennedy, R. Eberhart, Particle swarm optimization, in: 1995 IEEE international conference on neural networks, IEEE, 1995, pp. 1942–1948.
[45] M. E. H. Pedersen, Good parameters for particle swarm optimization.
[46] Jørgen Krabbenhøft, Shallow Water Tuned Liquid Dampers: Modeling, simulation and experiments, Ph.D. thesis, 2011.
[47] I. Kavrakov, A. Kareem, G. Morgenthal, Comparison metrics for time-histories: Application to bridge aerodynamics 146 (2020) 04020093.
[48] H. Sockel (Ed.), Wind-Excited Vibrations of Structures, volume v. 335 of *CISM International Centre for Mechanical Sciences Ser*, Springer Wien, Vienna, 2014.
[49] A. K. Chopra, Dynamics of structures: Theory and applications to earthquake engineering / Anil K. Chopra, Prentice Hall and London : Prentice-Hall International, Upper Saddle River, NJ, 2nd ed. edition, 2001.
[50] K. Dziedziech, A. Ghosh, J. Iwaniec, B. Basu, W. J. Staszewski, T. Uhl, Analysis of tuned liquid column damper nonlinearities, Engineering Structures 171 (2018) 1027–1033.
[51] C. Williamson, R. Govardhan, A brief review of recent results in vortex-induced vibrations, Journal of Wind Engineering and Industrial Aerodynamics 96 (2008) 713–735.
[52] International Organization for Standardization, Iso 6897 : Guidelines for the evaluation of the response of occupants of fixed structures, especially buildings and off-shore structures, to low-frequency horizontal motion (0.063 to 1 hz), 1984.
[53] International Organization for Standardization, Iso 2631-1 : Mechanical vibration and shock - evaluation of human exposure to whole-body vibration - part 1: General requirements, 1997.
[54] International Organization for Standardization, Iso 10137:2007 - bases for design of structures - serviceability of buildings and walkways against vibrations, 2007.
[55] Y. Tamura, S. Kawana, O. Nakamura, J. Kanda, S. Nakata, Evaluation perception of wind-induced vibration in buildings, Proceedings of the Institution of Civil Engineers - Structures and Buildings 159 (2006) 283–293.
[56] L.-L. Chung, Y.-A. Lai, C.-S. Walter Yang, K.-H. Lien, L.-Y. Wu, Semi-active tuned mass dampers with phase control, Journal of Sound and Vibration 332 (2013) 3610–3625.
[57] L.-L. Chung, L.-Y. Wu, H.-H. Huang, C.-H. Chang, K.-H. Lien, Optimal design theories of tuned mass dampers with nonlinear viscous damping, Earthquake Engineering and Engineering Vibration 8 (2009) 547–560.
[58] G. Morgenthal, J. H. Walther, An immersed interface method for the vortex-in-cell algorithm, Computers & Structures 85 (2007) 712–726.
[59] Guido Morgenthal, Aerodynamic Analysis of Structures Using High-resolution Vortex Particle Methods, Phd thesis, University of Cambridge, 2002.
[60] W. H. Melbourne, T. R. Palmer, Accelerations and comfort criteria for buildings undergoing complex motions, Journal of Wind Engineering and Industrial Aerodynamics 41 (1992) 105–116.

Appendix A

The model for showcasing VIV-type excitation for narrow-band response is selected as a harmonic force replicating the resonant shedding forces that could occur across-wind.

Following the Eurocode [35], the cross-wind amplitudes can be assessed through the characteristic maximum displacement, with Scruton number (Sc) among the terms which describe the damping of the structure. Vortex shedding criteria is considered if the resonant wind speed (U_{res}) for a specific mode is:

$$U_{res,i} < 1.25U, \tag{17}$$

where U is the characteristic 10 min mean wind speed where the vortex shedding occurs.
The vortex shedding action can be expressed as the inertia force acting perpendicular to the wind direction along with a certain correlation height of the structure:

$$F_w(z) = m(z)(2\pi f_i)^2 \phi_i(z) y_{max}, \tag{18}$$

where $m(z)$ is the vibrating mass per unit length [kg/m], f_i is the frequency of the structure of the i^{th} mode with its associated mode shape, ϕ_i, normalized at 1 with respect to the maximum displacement. The first frequency of the structure will be considered; therefore, the maximum displacement will occur at the tip of the chimney according to

the first mode shape. The calculation of cross-wind amplitude is calculated using approach 1, according to EC1:1-4 (Annex E.1.5.2)[35]:

$$y_{max} = \frac{KK_w c_{lat} D}{\mathrm{St}^2 \mathrm{Sc}}, \quad \mathrm{Sc} = \frac{2\delta m_e}{\rho D^2}, \tag{19}$$

where K is the mode shape factor, K_w is the effective correlation length factor, c_{lat} is the lateral force coefficient, St is the Strouhal number, expressed as a dimensionless number to describe the oscillating flow. Furthermore, δ is the logarithmic decrement of total damping, m_e is the equivalent mass per unit length for the sought mode, ρ is the air density under vortex shedding conditions, D is the width of the cross-section. Finally, the vortex shedding forces are applied to the structure along the correlation length (L_c).